EVAPORATIVE COOLING OF TRAPPED ATOMS

WOLFGANG KETTERLE AND N. J. VAN DRUTEN
Department of Physics and Research Laboratory of Electronics
Massachusetts Institute of Technology, Cambridge, Massachusetts

I. Introduction 181
II. Theoretical Models for Evaporative Cooling 184
A. General Scaling Laws 184
B. The Speed of Evaporation and Loss Processes 186
C. Models 193
D. The Dimension of Evaporation 197
E. The Number of Collisions for Thermalization 199
F. The Number of Collisions to Bose–Einstein Condensation 200
G. Desirable Extensions of the Models 200
III. The Role of Collisions for Real Atoms 201
A. Elastic and Inelastic Collisions 201
B. Atoms for Evaporative Cooling 203
C. Enhanced Relaxation in the Condensate 206
D. Special Topics 207
IV. Experimental Techniques 209
A. Precooling 209
B. Conservative Traps 212
C. Laser Cooling inside Conservative Traps 216
D. Adiabatic Compression 217
E. Evaporation Techniques 218
V. Summary of Evaporative Cooling Experiments 227
A. Hydrogen 227
B. Alkali Atoms 228
C. Comparison 229
VI. Outlook 229
References 231

I. Introduction

Evaporation is a well-known phenomenon in everyday life. It describes the conversion of liquid to the gaseous state. It either happens as a slow process, e.g., when a wet surface dries, or can be forced by means of heat or ventilation. In a more abstract sense, evaporation describes the process of energetic particles leaving a system with a finite binding energy. This

ISBN 0-12-003837-4

happens naturally since there are always high energy particles in the tail of the Maxwell–Boltzmann distribution. This process results in cooling: Since the evaporating particles carry away more than their share of thermal energy, the temperature of the system decreases. Due to the lower temperature, the evaporation process slows down, unless evaporation is forced by modifying the system in such a way that less energetic particles can escape from the system.

Evaporative cooling cools a cup of coffee, is used to cool apples by overtree sprinkling (Evans *et al.*, 1995), and is employed in technical water coolers (Berman, 1961). Stars evaporate from globular clusters (Spitzer, 1987). Evaporating neutrons carry away mega–electron volts of excitation energies of compound nuclei (Nolan and Twin, 1988). On the other end of the scale, at energies of pico–electron volts, evaporative cooling has led to the coldest temperatures ever observed in the universe: submicro-Kelvin temperatures generated in atom traps.

The last example is the subject of this chapter: evaporative cooling of trapped neutral atoms. The history of this technique is only a little bit shorter than the history of neutral atom trapping. In 1985, the year of the first realization of a trap for neutral atoms (Migdall *et al.*, 1985), Harald Hess (1985, 1986) suggested evaporative cooling as an efficient way to cool trapped atoms with the goal of achieving Bose–Einstein condensation. The original suggestion focused on trapped atomic hydrogen, but in 1994 this technique was extended to alkali atoms by combining evaporative cooling with laser cooling (Davis *et al.*, 1994; Petrich *et al.*, 1994b). It was the key technique to achieve Bose–Einstein condensation (BEC), a long-sought goal in atomic physics (Anderson *et al.*, 1995; Bradley *et al.*, 1995; Davis *et al.*, 1995b).

The recent observations of Bose–Einstein condensation showed dramatically the potential of evaporative cooling. Through evaporative cooling, phase-space density could be increased by six orders of magnitude in these experiments. Evaporative cooling was used to reach temperature and densities that were unprecedented for trapped atoms, and greatly exceeded what had been reached before by laser cooling. It should be noted that laser cooling has recently broken the recoil limit in three dimensions (3D) (Lawall *et al.*, 1995, Lee *et al.*, 1996), and reached extremely cold temperatures of 3 nK in 1D (Reichel *et al.*, 1995). However, none of these optical sub-recoil techniques have been realized so far at high densities ($>10^{12}$ cm^{-3}). The current density limitations are caused by absorption of light, radiation trapping, and excited state collisions. They might be avoided in dark optical traps which are being pursued theoretically (Dum *et al.*, 1994; Pellizzari and Ritsch, 1995) and experimentally (Hemmerich *et al.*, 1995; Davidson *et al.*, 1995).

What makes evaporative cooling so attractive is not only its simplicity, but also that it works over a wide range of temperatures and densities. The major requirement for the application of evaporative cooling is that the thermalization time be short compared with the lifetime of the sample. The lifetime might be technically determined by loss or heating processes of the atom trap, or it could be intrinsically limited by inelastic collisions ("bad collisions"). Eventually, since elastic collisions ("good collisions") are necessary for evaporative cooling, it is the ratio of good to bad collisions that sets the limit to evaporative cooling. This limit depends on the atomic species, as will be discussed in Section III, but for favorable species such as alkali atoms, the fundamental temperature limit is in the pico-Kelvin range. To overcome all technical limitations and reach this fundamental limit of evaporative cooling remains a formidable challenge.

An often-mentioned disadvantage of evaporative cooling is the loss of atoms. However, as discussed in Sections II and V, the efficiency of evaporative cooling is quite high. In recent experiments, phase-space density increases of six orders of magnitude were accomplished by losing only a factor of about 1000 in the number of atoms. Although the latter reduction is substantial, it can be compensated for by relatively straightforward improvements in loading the trap that can result in orders of magnitude higher numbers of atoms. Evaporative cooling is now an established cooling technique, and this will spur major efforts to get larger samples of trapped atoms—evaporative cooling allows transformation of higher initial numbers into higher final densities and lower temperatures.

Experiments on evaporative cooling have gone through rapid recent development. In the last few years, novel traps have been developed for the purpose of evaporative cooling, and novel ways of evaporating atoms were realized. We summarize these advances in Section IV. Equally important was the development of novel techniques to diagnose dense and cold samples of trapped atoms, but the description of these is beyond the scope of this chapter.

The process of evaporative cooling has been the subject of several theoretical studies, which we summarize in Section II. Evaporative cooling is a relatively simple classical process. Therefore, its theoretical foundation is well established. Some future research may address optimization of the cooling process and verification of models. However, we expect evaporative cooling to be mainly a tool to obtain colder and denser samples of trapped atoms. There is considerable hope of discovering new physics at ultralow temperatures, and the observation of Bose–Einstein condensation in dilute atomic gases might be just the first step. However, in this chapter, we will not discuss experiments that become possible through evaporative cooling; rather, we concentrate on the cooling process itself.

Previous review papers on evaporative cooling have focused on spin polarized hydrogen, the only gas that was cooled by this technique prior to 1994. The older reviews (Greytak and Kleppner, 1984; Silvera and Walraven, 1986) describe properties of spin polarized hydrogen in depth, and treat relaxation/recombination processes exhaustively. The latest reviews of the leading groups focus on wall-free confinement, evaporative cooling, and optical diagnostics (Walraven and Hijmans, 1994; Greytak, 1995; Walraven, 1996; Silvera and Reynolds, 1992; Silvera, 1995a, b).

We have attempted to give a complete guide to the relevant topics, and we hope that our work contributes to the successful cross-fertilization between the spin-polarized-hydrogen and laser-cooling communities. Most parts of this chapter are meant as an introduction to further study of the many references given. There are three topics where we feel that we have provided additional details or aspects not yet covered in the literature: a semiquantitative, comprehensive discussion of evaporative cooling both in hydrogen and alkalis (Sections II.A and B), a detailed discussion of rf-induced evaporation (Section IV.E), and a comparison among all experiments done so far on evaporative cooling (Section V).

II. Theoretical Models for Evaporative Cooling

A. General Scaling Laws

Several models describing the evaporative cooling process have been published. However, as we discuss here and in Section II.B, most of the dynamics of evaporative cooling is model independent and follows from simple considerations.

First, evaporative cooling happens on an exponential scale: Within a certain time interval (naturally measured in units of collision times or relaxation times), all relevant parameters (number of atoms, temperature, density) change by a certain factor. The characteristic quantities for the evaporation process are therefore logarithmic derivatives such as

$$\alpha = \frac{d(\ln T)}{d(\ln N)} = \frac{\dot{T}/T}{\dot{N}/N} \tag{1}$$

or, if evaporative cooling is described as a process with finite steps (Davis *et al.*, 1995c),

$$\alpha = \frac{\ln(T'/T)}{\ln(N'/N)} \tag{2}$$

where $T' = T + \Delta T$ and $N' = N + \Delta N$. (We are mainly following the notation of Walraven, 1996, which is the most comprehensive previous review article on the theory of evaporative cooling). If α is constant during the evaporation process, the temperature drops at $T(t)/T(0) = [N(t)/N(0)]^{\alpha}$. In a power law potential in d dimensions, $U(r) \propto r^{d/\delta}$, all relevant quantities scale as $[N(t)/N(0)]^{x}$ during evaporative cooling, where x depends only on δ and α. δ is defined in such a way that the volume scales as T^{δ}. All other quantities are products of powers of temperature, number, and volume, and their scaling is listed in Table I. Note that $\delta = 3$ for a 3D linear potential, $\frac{3}{2}$ for a 3D harmonic potential (generally anisotropic), and 0 for a box potential. As long as we are interested in scaling laws, it does not matter whether density is peak density or some form of average density. Phase space density D is defined as $n\lambda_{\mathrm{dB}}^3$ with the thermal de Broglie wavelength $\lambda_{\mathrm{dB}} = \sqrt{2\pi\hbar^2/mkT}$ for an atom with mass m. D is identical to the quantum occupancy number of the lowest state, as long as $D \ll 1$. Bose–Einstein condensation occurs for bosonic atoms when $D > 2.612$ (Huang, 1987).

The key parameter of the whole cooling process is α, which expresses the temperature decrease per particle lost. Technically, evaporation is controlled by limiting the depth of the potential to ηkT. The average energy of the escaping atoms is $(\eta + \kappa)kT$, where κ is a small number usually between 0 and 1, depending both on η and on the dimension of the evaporation (discussed later). For a qualitative discussion, we can ignore κ or approximate it by 1, especially in the case of large η.

For large η, the energy distribution of the trapped atoms is close to a Boltzmann distribution (to be discussed) with an average energy of $(\delta + \frac{3}{2})kT$ (assuming 3D motion), and there is a simple relation between

TABLE I
SCALING LAWS FOR EVAPORATIVE COOLING IN A d-DIMENSIONAL POTENTIAL $U(r) \propto r^{d/\delta}$

Quantity	Exponent[a], x
Number of atoms, N	1
Temperature, T	α
Volume, V	$\delta\alpha$
Density, n	$1 - \delta\alpha$
Phase-space density, D	$1 - \alpha(\delta + 3/2)$
Elastic collision rate, $n\sigma v$	$1 - \alpha(\delta - 1/2)$

[a] Each quantity scales as N^x, where N is the number of trapped particles.

the average energy of an escaping atom and α:

$$\alpha = \frac{\eta + \kappa}{\delta + 3/2} - 1 \tag{3}$$

This expression has an obvious meaning: α is a dimensionless quantity, characterizing how much more than the average energy $(\delta + \frac{3}{2})kT$ is removed by an evaporating atoms. These considerations show that in principle there is no upper bound for α or the efficiency of evaporative cooling. This is demonstrated by the following extreme example: With an extremely large η, one just has to wait for the event that one particle has all the energy of the system. Evaporating a single particle then cools the whole system to zero temperature. Unfortunately, this cooling strategy would take an almost infinite amount of time.

Therefore, efficiency of evaporation, and comparison between different trap geometries, can only be made if the trade-off between efficiency and cooling speed is considered. This is done by specifying loss mechanisms that are unavoidable in practice.

B. The Speed of Evaporation and Loss Processes

The considerations in the previous subsection focused on temperature decrease in evaporation as a function of the number of particles left. We now want to extend the discussion and consider the speed of evaporation, i.e., introduce time as a parameter. The situation we have in mind is forced evaporation at a constant η parameter; i.e., the threshold for evaporation is lowered in proportion to the decreasing temperature. Constant η ensures that the energy distribution is only rescaled during the cooling and does not change its shape. This assumption is reasonably well fulfilled in experiments.

We can easily obtain an analytical expression for the rate of evaporation in the following situation: We consider particles at density n_0 in a box potential, and we assume that η is large. The rate of evaporating atoms can then be obtained as follows: In an untruncated Maxwell–Boltzmann distribution, almost every collision involving an atom in the high energy tail removes the atom from the high energy tail. By detailed balance, elastic collisions produce atoms with energy larger than ηkT at a rate that is simply the number of atoms with energy larger than ηkT divided by their collision time. For a large value of η, the rate of evaporation in a truncated Boltzmann distribution is identical to the production rate of atoms with energy larger than ηkT in the untruncated distribution.

The velocity of atoms with energy ηkT is $\sqrt{2\eta kT/m} = \sqrt{\pi\eta}\,\bar{v}/2$ where $\bar{v}$ denotes the average thermal velocity. For large η, the fraction of atoms

with energy larger than ηkT approaches $2e^{-\eta}\sqrt{\eta/\pi}$. The rate of evaporating atoms is thus

$$\dot{N} = -Nn_0\sigma\bar{v}\eta e^{-\eta} = \frac{-N}{\tau_{ev}} \tag{4}$$

where we have introduced the elastic collision cross section σ and the time constant for evaporation τ_{ev}. Its ratio to the elastic collision time τ_{el} is expressed by $\lambda = \tau_{ev}/\tau_{el}$. Using $1/\tau_{el} = n_0\sigma\bar{v}\sqrt{2}$, where $\bar{v}\sqrt{2}$ is the average relative velocity between two atoms, we obtain, in the limit of large η,

$$\lambda = \frac{\sqrt{2}\,e^{\eta}}{\eta} \tag{5}$$

This expression is also valid for any power law potential in the limit of large η (Walraven, 1996), where n_0 is now the peak density. This last point is easily explained: Evaporation is a local phenomenon where each volume element can be regarded as a square well (Luiten *et al.*, 1996). For large η, the behavior is independent of the potential because the smaller threshold for evaporation for volume elements further outside in the cloud is, at least in leading order, compensated for by the lower local density. For arbitrary η, λ can be expressed analytically by generalized gamma functions, which are obtained from a collision integral for the truncated Boltzmann distribution (Luiten, 1993; Walraven, 1996; Luiten *et al.*, 1996).

The quantity $1/\tau_{el}$ is the elastic collision rate in the center of the trap. The cloud-averaged collision rate of one atom is smaller by a factor of $2\sqrt{2}$ in a parabolic trap, 8 in a linear trap. The event rate of collisions is smaller by another factor of 2 because each collision involves two atoms.

1. *Runaway Evaporation*

For alkali atoms, where the dominant loss mechanism is background gas collisions, an important criterion for sustained evaporation is to maintain or increase the elastic collision rate, $n\sigma v$. From Table I and Eq. (4), it follows that the elastic collision rate varies as

$$\frac{d(n\sigma v)}{dt}\Big/ n\sigma v = \frac{1}{\tau_{el}}\left(\frac{\alpha(\delta - 1/2) - 1}{\lambda} - \frac{1}{R}\right) \tag{6}$$

In the temperature range of interest, σ is the s-wave cross section and is independent of temperature. R is the number of elastic collisions per trapping time (also called the ratio of good to bad collisions): $R = \tau_{loss}/\tau_{el}$, where τ_{loss} is the time constant for trap loss due to background gas

collisions. Evaporation at constant or increasing collision rate ("runaway evaporation") requires

$$R \geq R_{\min} = \frac{\lambda}{\alpha(\delta - 1/2) - 1} \tag{7}$$

Figure 1 shows this minimum number of elastic collisions per trapping time. The figure includes plots based on the simple expressions for α (Eq. 3) and λ (Eq. 5), which are only valid for large η, and plots using the results of the more elaborate treatment of the Amsterdam group (Walraven, 1996; Luiten *et al.*, 1996).

The advantage of the linear confinement is clearly visible in Fig. 1. For the optimum choice of η, runaway evaporation in the linear trap occurs at a three to four times smaller ratio of good to bad collisions than in the parabolic trap. Qualitatively, one can understand this effect as a compression effect of the linear potential: In a potential $U(r) = U'r$, a cloud of temperature T has a size kT/U'. The same size is obtained by a harmonic confinement $U(r) = U''r^2/2$ with $U'' = U'^2/kT$. This means that evaporation in a linear potential is similar to evaporation in a harmonic potential with a force constant that is varied inversely proportional to the temperature. This compression greatly increases the density and elastic collision rate.

In the absence of any loss process ($R = \infty$), the minimum η for runaway evaporation is determined by

$$\alpha > \frac{1}{\delta - 1/2} \tag{8}$$

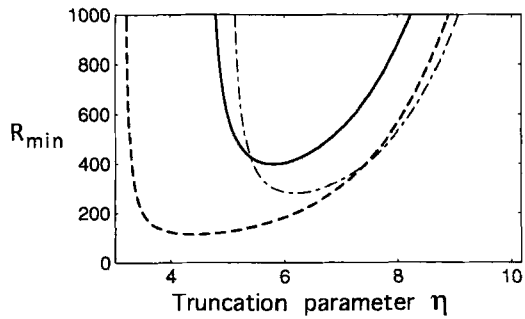

FIG. 1. The minimum ratio $R_{\min}$ of good to bad collisions needed for runaway evaporation, versus the truncation parameter η, Eq. (7). Plots are shown for parabolic (solid line) and linear (dashed line) potentials. The curves were calculated using the Amsterdam model. The dash–dotted line is obtained for a parabolic potential by using the approximations in Eqs. (3) and (5) for α and λ.

Equation (3) is not valid for such small η, and using a more accurate formula (Eq. (145) of Walraven, 1996) one obtains $\eta = 3.2$ and 4.6 for $\delta = 3$ and $\frac{3}{2}$, respectively.

The increase of phase space density with time is given by

$$\beta = 100\tau_{el}\frac{d}{dt}(\log_{10} D) = \frac{100}{\ln 10}\left(\frac{\alpha(\delta + 3/2) - 1}{\lambda} - \frac{1}{R}\right) \qquad (9)$$

β was normalized so that it gives the phase-space density increase (in orders of magnitude) per 100 elastic collision times. In Fig. 2, β is plotted versus the truncation parameter η for various ratios R of good to bad collisions. β becomes negative for small R and large η because slow evaporative cooling cannot compensate for fast losses due to background gas collisions. β reaches a maximum for low values of η: By rapid evaporation of atoms, a very large time derivative of D is possible; however, the density decreases, R becomes small, and the cooling process slows down and becomes inefficient.

2. *Maximizing Phase-Space Density*

Walraven (1996) has compared the efficiency of evaporation in different power law potentials by comparing the α parameter for certain evaporation strategies. However, α describes only the change in temperature. If we regard evaporation in a linear potential as analogous to evaporation in a harmonic potential with continuous adiabatic compression, we realize that α does not provide the most meaningful comparison, because adia-

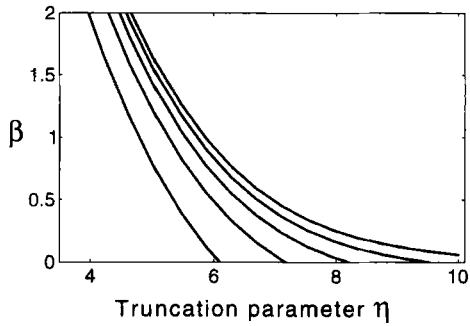

FIG. 2. Logarithmic phase-space density increase β per 100 elastic collision times, Eq. (9), versus the truncation parameter η. The ratio of good to bad collisions R is infinite (upper line), 500, 200, 100, and 50 (lower line), respectively. The potential is a 3D parabolic potential, and α and λ were obtained from the Amsterdam model.

batic compression trades in temperature against density. We therefore now focus on phase-space density D, which is invariant with respect to adiabatic changes of the potential.

By analogy with Eq. (6) we find the relative increase in phase space density with decreasing number N:

$$\gamma = -\frac{d(\ln D)}{d(\ln N)} = \frac{\alpha(\delta + 3/2)}{1 + \lambda/R} - 1 \tag{10}$$

Figure 3 plots γ versus η for different values of R for a linear and a parabolic potential. As expected, for long trapping times (large R), the optimum γ is realized with large truncation parameters η. The efficiency γ of the evaporation process is higher in a parabolic trap than in a linear trap. However, this reflects only the situation at the same value of R. For the example shown in Fig. 3 with $R = 200$, the linear trap operates in the runaway regime, whereas in the harmonic case the elastic collision rate is decreasing. This mean that the process in the linear trap works with increasing R and therefore increasing γ, whereas the trend is opposite in the harmonic trap (see Section II.B.3).

The most important figure of merit of evaporative cooling in atom traps is to achieve the maximum increase in phase-space density with the smallest loss in the number ("to reach BEC with the largest number of atoms possible"). This would mean that the goal is to achieve the largest value of the global parameter

$$\gamma_{\text{tot}} = \frac{\ln(D_{\text{final}}/D_{\text{initial}})}{\ln(N_{\text{final}}/N_{\text{initial}})} \tag{11}$$

This global parameter is optimized by optimizing γ (Eq. 10) at any moment. (This was first brought to our attention by R. Hulet). To explain this, we first note that the elastic collision rate at any moment can be expressed by the phase-space density and the number of atoms:

$$n\sigma v \propto D^{(\delta-1/2)/(\delta+3/2)} N^{2/(\delta+3/2)} \tag{12}$$

Then we divide the increase in phase-space density in many small steps of size ΔD. The efficiency γ of the second step is optimized by maximizing R (see Eq. (10)). According to Eq. (12), this is achieved by maximizing the number of atoms left after the first step. As a result, following an evaporation path that maximizes γ at any given point maximizes γ_{tot} and, thus, the number of atoms left at the final phase-space density.

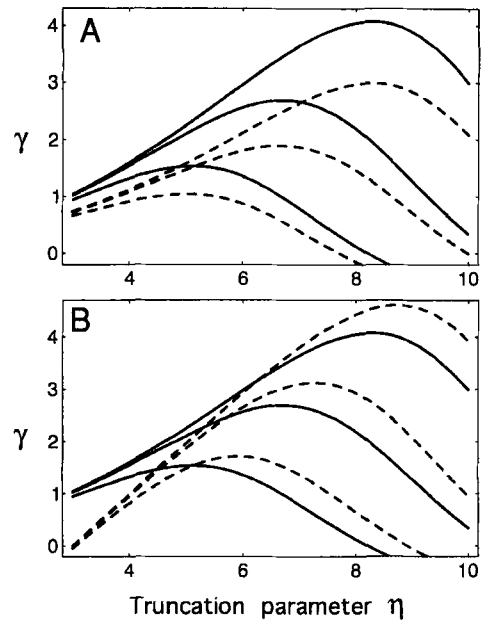

FIG. 3. The efficiency parameter of evaporative cooling, $\gamma = d(\ln D)/d(\ln N)$, versus the truncation parameter η. (A) Comparison between a 3D parabolic potential ($\delta = \frac{3}{2}$, solid lines) with a linear potential ($\delta = 3$, dashed lines). γ was calculated using Eq. (10), where α and λ were obtained from the Amsterdam model. (B) γ for a 3D parabolic potential; the solid lines are identical to those in (A), and the dashed lines are obtained by using the approximations in Eqs. (3) and (5) for α and λ. In each case, three different lines are given, for ratio of good to bad collisions R of 5000 (upper lines), 1000, and 200 (lower lines), respectively.

The same conclusion applies for cooling of atomic hydrogen, where the dominant loss process is inelastic binary collision (to be discussed). R is then independent of density and proportional to $\sqrt{T}$, resulting in

$$R \propto D^{-1/[2(\delta+3/2)]} N^{1/[2(\delta+3/2)]} \tag{13}$$

Again, optimizing N in one step maximizes R and, therefore, γ for the following step.

There is one major difference between the loss due to background gas collisions and that due to inelastic collisions. Inelastic collisions heat up the sample because they happen most frequently in regions of high density, where the potential energy is small. As a result, atoms lost due to inelastic collisions carry away less than their share in total energy, thus increasing the average energy of the trapped atoms. This effect is quantitatively discussed by Walraven (1996) and decreases the effective α, which ex-

presses the average energy of a lost particle. Actually, α even changes sign as a function of temperature when the heating due to dipolar relaxation dominates over the evaporative cooling. The criterion $\alpha = 0$ determines the lowest temperature that can be achieved in evaporative cooling due to relaxation heating, whereas a model considering only background gas collisions allows cooling to arbitrarily small temperatures.

3. *Strategies for Evaporation Cooling*

It might appear that the two previous subsections on phase-space density increase and runaway evaporation describe different strategies or even conflicting goals. We now want to discuss qualitatively how they depend on each other and emphasize the major difference between evaporative cooling in alkalis and in atomic hydrogen.

The ultimate goal is the achievement of high phase-space densities. As was pointed out, maximizing γ is the optimum strategy for this goal. However, for small R, γ becomes negative; i.e., no increase in phase-space density is possible. Therefore, a phase-space density increase can only be sustained as long as R is larger than a critical value.

For loss due to background gas collisions (the dominant limitation for alkalis), R changes according to Eq. (6), or equivalently,

$$-\frac{d(\ln R)}{d(\ln N)} = \frac{\alpha(\delta - 1/2)}{1 + \lambda/R} - 1 \tag{14}$$

R varies exponentially with $1/N$, with the exponent given by the right hand side of Eq. (14). If the exponent is negative at some point during the cooling (even for optimized η), R decreases, resulting in an even more negative exponent later on. The consequence is an accelerated decrease of R and an accelerated reduction of the efficiency parameter γ, until eventually γ reaches zero and no further increase in phase-space density is possible. Work in alkali systems concentrated on realizing an initial situation with a sufficiently large R, so that R increased during evaporation. In principle, cooling with a (slowly) decreasing R is possible, as long as the desired phase-space density is reached before γ becomes zero. However, when the threshold of runaway evaporation is reached, R stays constant or increases. This guarantees both fast and efficient cooling to very high phase-space densities. The phase-space density increase is only limited by the onset of other loss processes such as three-body recombination and dipolar relaxation, which inevitably reduce R and throttle the cooling process.

In atomic hydrogen, the situation is quite different. All experiments in atomic hydrogen were done in a cryogenic environment where background

gas collisions were negligible, and the dominant loss mechanism was inelastic binary collisions. R is independent of density and decreases proportionally to $\sqrt{T}$. Runaway or increasing collision rates speed up the cooling process, but in contrast to alkali atoms, they do not increase R nor improve the efficiency of evaporative cooling. In all experiments, the initial temperature, and therefore R, was large enough to allow efficient cooling in the beginning. However, during the cooling process the efficiency decreased, and the highest phase-space densities were reached when either γ became small and/or the number of atoms in the sample reached the detection limit.

We want to add one additional comment with regard to adiabatic compression. Adiabatic compression increases both temperature and density and therefore always increases R. As a result, the increase in phase-space density after adiabatic compression is always superior, and the optimum strategy is to use the tightest confinement possible. This strategy only finds its limitations when three-body recombination sets in, or when the collision time for an evaporating atom becomes comparable with its escape time from the trap. In the latter case, λ in Eq. (10) increases with density.

C. Models

In the previous subsections, we have sketched a semiquantitative picture of the evaporation process, which was partly a simplification and partly an extension of models by other authors. It was mainly stimulated by work of the Amsterdam group (Walraven, 1996; Luiten *et al.*, 1996) and our own previous work (Davis *et al.*, 1995c). In this section, we will summarize the different efforts aimed at modeling evaporative cooling.

1. *Amsterdam*

The Amsterdam group modeled evaporative cooling within a kinetic theory involving a numerical solution of the Boltzmann equation. These results confirmed that the energy distribution can be very well approximated by a truncated Boltzmann distribution (Luiten *et al.*, 1996). This assumption of quasi-equilibrium has been often used in previous work, but it had not been thoroughly checked before. Subsequently, a closed set of differential equations for evaporative cooling was derived under the assumption of a truncated Boltzmann distribution, i.e., that all particles with energy larger than ηkT leave the trap.

In particular, the Amsterdam group has exactly calculated the collision integral for the number of particles produced with energy larger than ηkT. For example, Eq. (140) of Walraven (1996) for $d(\ln N)/d(\ln T)$ replaces our Eq. (3) for α. Our κ is expressed by their term $(1 - X_{ev}/V_{ev})$. The average energy $\delta + \frac{3}{2}$ is generalized to their expressions $\tilde{\gamma} + \frac{3}{2}$ and C_i/Nk, which differ only when the truncation of the Boltzmann distribution becomes important. Furthermore, when the threshold energy for evaporation is ramped down (forced evaporation), the average energy of the evaporating atoms is reduced from $(\eta + \kappa)kT$, because atoms are now "shaved" away at an energy ηkT. This results in a "spilling" correction that is proportional to κ, the difference in energy between a "truly evaporated" and a "spilled" atom (see Walraven, 1996, for details). In the language of that paper, our λ parameter would be expressed as $\sqrt{2}(1 - \tilde{\xi}\tilde{\alpha})e^{\eta}(V_c/V_{ev})$. The nice feature of the Amsterdam treatment is that most of the final expressions, although seemingly complicated, have been solved analytically in terms of generalized gamma functions. Analytical expressions were not only derived for power law potentials, but also for a potential that is a very good approximation to the Ioffe–Pritchard configuration, which is frequently used for trapping hydrogen and alkalis (Luiten *et al.*, 1996).

This model included dipolar relaxation as a loss and heating mechanism, and it was used to discuss the prospects of cooling trapped atomic hydrogen into BEC. They concluded that BEC can be obtained in magnetically trapped atomic hydrogen, and that phase-space density can be increased down to temperatures of 30 nK (Luiten *et al.*, 1996). However, below 2 μK, the density decreases due to the strong truncation of the Boltzmann distribution, which is necessary to cool against the loss and heating due to dipolar relaxation.

2. *Davis and Coworkers (MIT)*

An analytical model for evaporation was presented earlier by our group (Davis *et al.*, 1995c). It approximated the evaporation process as a discrete series of truncation and rethermalization processes, and it arrived at simple analytical results. These were used to discuss the threshold for runaway evaporation for different potentials.

This model described a situation that is not directly realized in the experiments. It assumed thermalization of the distribution (both in velocity and position space) before the next truncation step, and it estimated that the time for rethermalization is several collision times. This situation would be realized in radiofrequency (rf)-induced evaporation when the rf

is pulsed on and off with an off time that is longer than the thermalization time.

In real experiments, the truncation is continuous. Still, the number of evaporated atoms can be approximated by an integral over the tail of the velocity distribution using detailed balance (see Section II.B). This argument shows the connection between the Amsterdam model and that of Davis *et al.*, which have the same asymptotic behavior in a box potential. For any other potential, however, there are discrepancies, because Davis *et al.* assumed replenishment of the wings of both the velocity and spatial distribution before the next truncation was performed. In the Amsterdam model, collisions fill up the empty states only within the spatially truncated cloud; the spatial wings are not involved in the evaporation process. In that sense, one might say that normal evaporation involves only velocity space, whereas the pulsed evaporation discussed by Davis *et al.* occurs in both velocity and position space. Furthermore, as was discussed, the time to replenish the tail of the velocity distribution depends on η and is faster than a collision time (by a factor $\sqrt{\pi\eta/8}$), whereas replenishment of the spatial tail takes longer. The time step in the model of Davis *et al.* was assumed to be several thermalization times and therefore corresponds to evaporation that is not forced at the maximum possible speed.

The major purpose of this discrete model was to obtain fully analytical expressions for the evaporation dynamics in the simple case of alkali atoms, where background gas collisions are the dominant loss mechanism. In Section II.B, we have extended the Amsterdam model to this situation and discussed runaway evaporation and the efficiency of evaporative cooling in the presence of background gas collisions. We feel that the present discussion is more realistic than our earlier treatment, and that the discrete model is mainly of pedagogical value because of its simplicity.

3. *Doyle and Coworkers (MIT)*

John Doyle and collaborators derived a set of coupled differential equations that described various cooling, heating, and loss processes and included adiabatic changes of the potential during the cooling process (Doyle *et al.*, 1991, 1994; Doyle, 1991). This was the first comprehensive model of evaporative cooling. The numerical solution of these equations agreed very well with the evaporative cooling experiments done at MIT. Furthermore, optimized trajectories in phase space were determined aiming at the highest final phase-space density for a given initial temperature and density combination. Those calculations predicted that it should be possible to reach BEC in hydrogen with initial conditions realized by the MIT group (Doyle, 1991).

The equations of Doyle *et al.* (1991, 1994) and Doyle (1991) neglected the spilling of particles due to forced evaporation, which was unimportant in the MIT experiments but is essential for the alkali experiments. It could easily be added to their formalism. The spirits of this model and of the Amsterdam model are very similar. The Amsterdam model can be regarded as a major extension of the work by Doyle *et al.* (1991, 1994) and Doyle (1991), especially because the predominately analytical treatment provides additional insight.

4. *Earlier Work*

For completeness and historical interest, we mention earlier work on modeling evaporative cooling. The concept of wall-free confinement and evaporative cooling of atomic hydrogen was conceived by Hess around 1983 or 1984, quite some time before it was published, and was discussed and refined by the MIT group. The original suggestion by Hess (1985, 1986) already discussed the interplay between cooling and dipolar heating and derived some of the scaling laws presented in Section II.A. He proposed that such a technique could cool and compress atomic hydrogen to attain Bose–Einstein condensation at a temperature of 30 μK.

Similar ideas were, probably independently, conceived by Lovelace *et al.* (1985) and Tommila (1986). They refer to Hess's abstract of his presentation at a meeting of the American Physical Society (APS) (Hess, 1985). Lovelace *et al.* proposed a dynamic trap in which dipolar relaxation would be absent. Tommila investigated the dynamics of evaporative cooling in linear, quadratic, and square potentials.

5. *Monte Carlo Simulations*

Very recently, two groups developed an elegant Monte Carlo trajectory technique that allowed an efficient solution of the classical kinetic equation (Holland *et al.*, 1996b; Wu and Foot, 1996). This technique solves the Boltzman equation directly without any assumptions such as partial equilibrium or the presence of a truncated Boltzmann distribution.

This method, similar to the "Monte Carlo wavefunction" approach in quantum optics, is claimed to be computationally much less intensive than the usual collision integral treatment. These calculations show good agreement with the calculations based on the truncated Boltzmann distribution (Luiten *et al.*, 1996). There are small differences, however, which are attributed to the deviation from the truncated Boltzmann distribution. Wu

and Foot (1996) showed that the axial and radial temperature during two-dimensional (see Section II.D) forced evaporation differ by up to 25%.

6. *Quantum Mechanical Models*

Several authors have studied a quantum mechanical three-level model that strips evaporative cooling to its bare bones (Holland *et al.*, 1996a; Wiseman *et al.*, 1996). These models were developed to describe a possible realization of an "atom laser" pumped by elastic collisions. The ground state is the single state that collects the cold atoms; collisions between atoms in the first excited state result in the necessary energy exchange; and the second excited state is sufficiently damped so that the high energy atoms are lost. The goal was to obtain a microscopic model for the accumulation of particles in the ground state, including quantum statistical effects. The influence of interactions on fluctuations of the occupation numbers in this simple model of evaporative cooling was studied by Quadt *et al.* (1996). The ideal Bose gas shows anomalous fluctuations of the ground state population in the framework of the grand-canonical ensemble (Greytak and Kleppner, 1984). Those fluctuations were shown to be suppressed in the presence of interactions.

D. The Dimension of Evaporation

Evaporative cooling relies on the selection of energetic particles that leave the trap. This selection can be based on the total energy E or on the energy for the motion in a particular direction, e.g., E_z. We call the selection one-dimensional if it is based on $E_z > \eta kT$, two-dimensional for $E_x + E_y > \eta kT$, and three-dimensional for $E > \eta kT$. This distinction is rigorous only for separable potentials. In the context of evaporative cooling the relevant timescale is the time between elastic collisions. Thus, if the ergodic mixing time is longer than the elastic collision time, the potential can be regarded as separable. This is the situation in many atom traps (Helmerson *et al.*, 1992b; Monroe *et al.*, 1993; Davis *et al.*, 1995b), where ergodic mixing of many seconds was observed, much longer than typical collision times of milliseconds to a second.

In the case of negligible ergodic mixing, the depletion of the high-energy tail of the distribution depends on the selection method. In the opposite case of fast ergodic mixing the distribution is depleted for total energy $E > \eta kT$, independent of the dimensionality of the selection. Since the dynamics of the evaporation are determined by the dimension of the depletion, we will call this the *dimension of evaporation.*

Most evaporative cooling experiments on hydrogen used evaporation over a saddle point of the potential which is a 1D selection scheme. Radiative evaporation using rf is a three-dimensional selection scheme in a dc magnetic trap. However, in the TOP trap, it is only two-dimensional, and if gravitational forces become essential, it is only one-dimensional (Section IV.E.4).

The problem with evaporation in lower dimensions is the dramatic reduction in efficiency, as was first discussed by Surkov *et al.* (1996) for an Ioffe–Pritchard (IP) trap. The reason is that a major fraction of the atoms that have enough total energy to escape collide with other atoms and lose the high excitation energy. Therefore, several "attempts" are necessary before an atom leaves the trap.

As long as there are no loss processes, this affects only the time for evaporation. However, if a time limitation is set by inelastic collision processes and background gas collisions, one- or two-dimensional evaporation strongly decreases the efficiency of evaporative cooling. This can be readily seen with Eq. (10). Since loss processes enter in the ratio λ/R, an increase in λ has an effect similar to a decrease in the ratio of good to bad collisions.

Surkov *et al.* (1996) compared axial and three-dimensional evaporation in the Ioffe–Pritchard trap. The rate of axial evaporation was smaller by a factor of 4η (η is typically between 5 and 10). Wu and Foot compared evaporative cooling in three and two dimensions and showed a scenario in which the trap depth was ramped down by a factor of 1000. The phase-space density increase in 3D evaporation was 20 times high than in 2D, and the fraction of the remaining atoms was three times higher (Wu and Foot, 1996).

The much lower efficiency of evaporation in lower dimensions follows from a simple geometric argument: In velocity space, the evaporating atoms are mainly from a shell with velocities between $\sqrt{2\eta kT/m}$ and $\sqrt{2(\eta+1)kT/m}$. This reflects that κ (Eq. 3) is about 1. The volume of this shell which has a z component of the velocity larger than $\sqrt{2\eta kT/m}$, is a factor of 4η smaller than the whole shell. Thus, λ is reduced by approximately this factor. In 2D evaporation, λ is reduced by a factor of $3\sqrt{\eta}/2$.

Keeping λ, the number of collisions per evaporating atom, as small as possible is particularly important for atomic hydrogen, where the evaporation is limited by the decrease of R with decreasing temperature. However, the only demonstrated method for 3D selection is rf-induced evaporation. This technique has not been demonstrated yet in a cryogenic environment.

We want to add a rather technical remark: If one compares 3D with 1D evaporation, one has to consider that κ, which determined the energy $(\eta + \kappa)kT$ of an evaporating atom, is no longer between 0 and 1, but larger. This is because atoms with a larger excess energy are less affected by the reduced dimension of evaporation. If the transverse and axial motion are separable, κ is about 1 plus the average energy along the transverse directions. The larger value of κ improves the α parameter. As a result, one should not compare 1D and 3D evaporation at the same η; rather, one should evaluate Eq. (10) for γ with the appropriately modified λ and α. This follows the spirit of our earlier suggestion: Comparison between different potentials and/or evaporation methods should use the efficiency of evaporation as defined in Eq. (10) as the figure of merit.

E. The Number of Collisions for Thermalization

Several authors have discussed the number of elastic collisions necessary for thermalization (Snoke and Wolfe, 1989; Snoke *et al.*, 1992; Monroe *et al.*, 1993; Davis *et al.*, 1995a; Coakley, 1996). This concept is important for evaporative cooling if one regards the evaporation process as a truncation–replenishment cycle (Davis *et al.*, 1995c). However, most models of evaporative cooling avoid the notion of thermalization by calculating the flux of evaporating atoms from the collision term of a Boltzmann equation. In any case, evaporative cooling creates a truncated and, therefore, nonthermal energy distribution, and the relaxation of this distribution to an equilibrium distribution is important, e.g., when the final temperature is determined at the end of the cooling process.

Snoke and Wolfe (1989) performed numerical quantum mechanical calculations on the relaxation of a nonthermal distribution and found that the distribution was indistinguishable from a thermal distribution after five collisions, independent of the nature of the nonthermal distribution.

Experimentally, elastic collision cross sections were determined by preparing a sample with different temperatures along the axial and radial directions and observing the equilibrium. In this way, the low temperature, elastic collision cross sections for cesium, sodium, and rubidium were determined (Monroe *et al.*, 1993; Davis *et al.*, 1995a; Newbury *et al.*, 1995). The number of elastic collisions for such a cross-sectional relaxation was numerically determined to be 2.7 (Monroe *et al.*, 1993). This result was later confirmed by an analytic solution of the Boltzmann transport equation (Newbury *et al.*, 1995) and also by a Monte Carlo trajectory calculation (Wu and Foot, 1996).

We have shown in Section II.A, using detailed balance arguments, that the high energy tail of the velocity distribution is replenished in one elastic

collision. Since the collision time for fast atoms enters, we arrive at the counterintuitive result that the higher the energy of the truncated tail is, the shorter is this replenishment time. This argument only applies to replenishment in velocity space; the thermalization of a spatially truncated cloud requires at least one oscillation period for the energetic atoms to reach the outer parts of the cloud, and it will eventually depend on the ergodicity of the trapping potential.

F. The Number of Collisions to Bose–Einstein Condensation

All the models discussed here show that evaporative cooling is a fast and efficient way to reduce the temperature of trapped atoms and increase the phase-space density. A possible scenario is as follows (see Figs. 2 and 3): harmonic potential, η parameter of 6, removal of 0.7% of the atoms per collision time, increase of phase-space density by a factor of 10^6 in 600 collision times, and a loss in the number by a factor of 100. Reduction of the η parameter to 5 gives the same phase-space density increase in half the number of collisions, but with 5 times fewer atoms left.

Since the phase-space density of laser-cooled atoms is typically 10^{-6} lower than is required for Bose–Einstein condensation (BEC), one can summarize the potential of evaporative cooling in the following way: About 500 collision times suffice to achieve BEC with 1% of the atoms remaining!

Real experiments have performed somewhat worse (Section V), probably due to nonoptimized cooling, lower dimension of the evaporation, and additional loss and heating processes. However, the few experiments done so far have already impressively confirmed the potential of evaporative cooling.

G. Desirable Extensions of the Models

The theoretical foundations of evaporative cooling are well established. The different models we have discussed describe the salient features of the evaporation process. Extensions in the following directions appear worthwhile:

1. The calculation of optimized trajectories in phase space. There are obviously trade-offs between efficiency and cooling time, and some detailed treatment is desirable.

2. So far, all models assume that all particles with a certain (1D or 3D) energy will escape. However, all methods of evaporation rely on spatial selection of atoms. Energetic atoms that are on circular orbits have a smaller outer turning point than atoms undergoing radial oscillations. Such

nonergodic effects reduce the efficiency of evaporative cooling. So far, only one theoretical paper has addressed this problem (Surkov *et al.*, 1996).

3. All models discuss evaporation in the dilute regime. Dilute means here collisionally thin, or that the mean free path is longer than the size of the sample. One consequence is that the products of inelastic collisions leave the sample without transferring their energy to other atoms. It is obvious that the dense limit is not advantageous for evaporative cooling and should be avoided by adiabatic expansion, but there is probably some trade-off involving efficiency, speed, and collisional mixing that ensures ergodicity.

4. Most models have treated the atomic motion classically, ignoring quantum statistical effects. For the description of the cooling process, this is justified because evaporative cooling has been used to increase the phase-space density by six orders of magnitude, whereas quantum statistical effects are only pronounced in the vicinity of BEC. However, the last stage of the cooling and the actual formation of a Bose condensate are a very interesting regime to study both theoretically (Stoof, 1995; Kagan, 1995) and experimentally. So far, only simplified three-level models have been formulated, which combine evaporative cooling with quantum effects (Holland *et al.*, 1996a; Wiseman *et al.*, 1996) (see Section II.C.6).

III. The Role of Collisions for Real Atoms

A. Elastic and Inelastic Collisions

Evaporative cooling is driven by elastic collisions. High density and the presence of collisions are therefore prerequisites for evaporative cooling. However, this means that inelastic collisions are unavoidable. We have already mentioned background gas collisions and dipolar relaxation as loss processes, and we wish to give a more systematic account of collision processes in this section. For a more comprehensive treatment of cold collisions, we refer to several review articles on this subject (Silvera and Walraven, 1986; Verhaar, 1995; Heinzen, 1995; Walker and Feng, 1994; Lett *et al.*, 1995).

In a magnetic trap, three kinds of inelastic collisions are relevant for evaporative cooling experiments: dipolar relaxation and spin relaxation, which are binary collisions, and three-body recombination (or dimerization). In an optical dipole trap (to be discussed), atoms can be trapped in the lowest hyperfine state, eliminating binary collisions as trap loss process. If atoms are trapped in the upper hyperfine state, hyperfine state changing collisions are important (Walker and Feng, 1994), and the loss processes

are similar to the situation in a magnetic trap. In this section, we focus on the most common situation of magnetically trapped samples.

An overview of the relevant collisional parameters for hydrogen and the alkalis is given in Table II. Spin relaxation has a rather large rate coefficient, typically 10^{-12} cm^3/sec. It involves an exchange of angular momentum between the electron spin and the nuclear spin. This process is usually important only after the initial loading of the trap and leads to a "self-purification" of the sample in the sense that there are only atoms left in a hyperfine state, which does not undergo spin relaxation. This usually happens in the first few seconds after loading a magnetic trap with atomic hydrogen (Greytak, 1995).

Spin relaxation is forbidden for a doubly spin polarized sample due to angular momentum conservation, and also in the upper (weak-field-seeking) sublevel of the lower hyperfine level (as long as kT is small compared with the ground state hyperfine splitting). However, spin-flips can still occur by coupling the spin angular momentum to the orbital angular momentum. This process, called dipolar relaxation, happens with a rate coefficient G_{dip} of typically 10^{-15} cm^3/sec, 1000 times smaller than spin relaxation. The rate coefficients for dipolar relaxation are similar for hydrogen and alkalis.

As for all inelastic processes, the rate coefficient G_{dip} is constant for temperatures approaching zero, whereas for elastic collisions the cross section σ approaches a constant. This means that in the limit of low temperature and low density (so that three-body recombination can be neglected) the ratio of good to bad collisions is given by $\sqrt{2}\,\sigma\bar{v}/G_{\text{dip}}$.

This ratio reaches unity at a characteristic temperature T_*:

$$kT_* = \frac{\pi m G_{\text{dip}}^2}{16\sigma^2} \tag{15}$$

This temperature represents a theoretical lower bound to the minimum temperatures attainable by forced evaporation. As shown by Luiten *et al.* (1996), the minimum temperature in a harmonic trap is about three times larger than T_*. The smallest temperature that can be reached by evaporative cooling with increasing density is approximately 2000 times larger. One might thus regard $1000T_*$ as the practical temperature limit of evaporative cooling.

The rate of three-body recombination is given by Ln^2, where L is the rate coefficient. In a simple picture, one can estimate the rate for three-body recombination as a (2 + 1) process, a collisional encounter between two atoms with a third one joining. This suggests a correlation between the elastic cross section and the rate for three-body recombination. Recent

TABLE II
COLLISION PARAMETERS[a]

Atom	$a_<$ (a_0)	$a_>$ (a_0)	G_{ex}[b] (cm^3/sec)	$G_{dip,>}$ (cm^3/sec)	$L_>$ (cm^6/sec)
^{1}H	absent	1.4[c]	2×10^{-13} [d]	10^{-15} [e]	10^{-38} [f]
^{7}Li	10[g]	-27.3 ± 0.8[h]		2×10^{-14} [q]	2.6×10^{-28} [i]
^{23}Na	92 ± 25[j]	45 to 185[g]	10^{-11} [k]	3×10^{-15} [k]	2.0×10^{-28} [i]
^{85}Rb	?[l]	-1000 to -60[m]		3×10^{-14} [r]	
^{87}Rb	?[l]	85 to 140[m]		10^{-15} [r]	4×10^{-30} [i]
^{133}Cs	?[n]	-1100 to -200[n]		10^{-16}–10^{-15} [p]	5×10^{-29} [p]

[a] Where available, the parameters have been taken for temperature $T \to 0$ and magnetic field $B \to 0$. The dependence on T and B is weak, except where indicated. Subscript $>$ indicates the $F = m_F = F_{max}$ low-field-seeking doubly polarized state; subscript $<$ refers to the low-field-seeking $F = -m_F = F_{max} - 1$ state.

[b] Spin exchange coefficient G_{ex}, typical value for a mixture of low-field-seeking states.

[c] Friend and Etters (1980).

[d] Stoof *et al.* (1988).

[e] van Roijen *et al.* (1988).

[f] Hess *et al.* (1984).

[g] Moerdijk and Verhaar (1994).

[h] Abraham *et al.* (1995).

[i] Moerdijk *et al.* (1996a).

[j] Davis *et al.* (1995a).

[k] Tiesinga *et al.* (1991). A recent, improved calculation gives $G_{dip,>} = 7 \times 10^{-15}$ cm^3/sec for sodium (Moerdijk and Verhaar, 1996). For the lower hyperfine state, recent calculations yield $G_{dip,<} \approx 10^{-16}$ cm^3/sec, at magnetic fields of a few gauss (Moerdijk and Verhaar 1996).

[l] Verhaar (1995).

[m] Gardner *et al.* (1995).

[n] Verhaar *et al.* (1993).

[p] Tiesinga *et al.* (1992).

[q] Moerdijk and Verhaar (1996).

[r] Boesten *et al.* (1996).

calculations show that this correlation exists (Moerdijk *et al.*, 1996a; Fedichev *et al.*, 1996b).

Three-body recombination was the limiting process in the attempt to reach quantum degeneracy in spin polarized hydrogen at temperatures of 500 mK (Greytak, 1995). Evaporative cooling at much lower temperature and density turned out to be the solution to avoid this process.

B. ATOMS FOR EVAPORATIVE COOLING

Three kinds of atoms have been used or discussed for evaporative cooling: atomic hydrogen, alkali atoms, and metastable helium. They show major differences in their collisional properties.

Atomic hydrogen is distinguished by an extremely small s-wave scattering length $a = 0.072$ nm (Friend and Etters, 1980) resulting in an elastic cross section $\sigma = 8\pi a^2 = 1.3 \times 10^{-15}$ cm^2. With a rate coefficient for dipolar relaxation of $G_{\text{dip}} = 1.0 \times 10^{-15}$ cm^3/sec (van Roijen *et al.*, 1988), the ratio of good to bad collisions at $T = 1$ mK is 800. Since trapping experiments for atomic hydrogen are always carried out in a cryogenic environment (the trap is loaded by cryogenic precooling of the atoms), the background gas pressure is extremely low, and the trapping time is usually determined by inelastic collisions among the trapped atoms themselves rather than by background gas collisions.

The rate for three-body recombination is extremely small for spin polarized atomic hydrogen. This reflects the fact that the lowest triplet state of the hydrogen molecule is repulsive, and three-body recombination is only possible through the weak interaction of the electron magnetic dipole moments. As a result, for most realistic situations, the major loss and heating process during evaporative cooling is dipolar relaxation (Fig. 4a).

In alkali vapors, the situation is very different. The s-wave scattering length is on the order of 5 nm, resulting (e.g., for Na) in an elastic cross section of 6×10^{-12} cm^{-2}, more than 1000 times larger than for hydrogen. The rate constant for dipolar relaxation is similar to that for atomic hydrogen (see Table II). As a result, the ratio of good and bad (binary) collisions is extremely high, e.g., for Na at 10 μK it is 24,000. Most evaporative cooling experiments on alkalis work at densities of at most 10^{12} to 10^{13} cm^{-3}. The time constant for loss due to dipolar relaxation is more than one minute, and it plays only a minor role for the evaporative cooling. However, the Na experiment at MIT realized densities of 10^{14} cm^{-3}, where inelastic collisions should be important. The rate constant L for three-body recombination is typically 10 orders of magnitude larger than for atomic hydrogen and is on the order of 10^{-28} cm^3/sec (see Moerdijk *et al.*, 1996a, for recent calculations for different atoms). Trap loss due to three-body recombination dominates for densities $n > G_{\text{dip}}/L$, which is typically 10^{13} cm^{-3}. At this density, the time constant for inelastic collisions is about 100 sec. That is why we expect that in most situations the trapping time is either limited by background gas collisions at low density, or by three-body recombination at high density (Fig. 4b). It is possible that dipolar relaxation will limit evaporative cooling of alkali atoms only if one attempts to cool samples at low density and extremely low background pressure.

Since dipolar relaxation is the dominant limitation for atomic hydrogen, early discussions on evaporative cooling in alkalis overly focused on this loss mechanism. One suggestion how to avoid this loss process was trap-

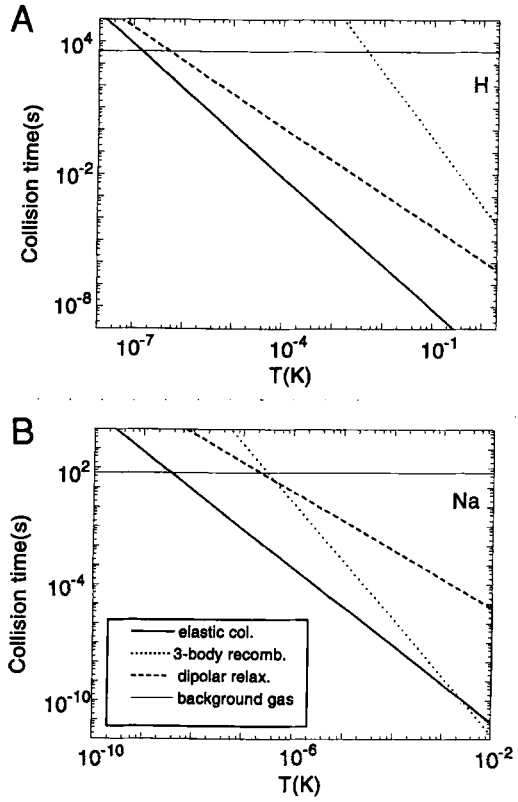

FIG. 4. Collision times for several elastic and inelastic processes, as a function of temperature, at the density needed for Bose–Einstein condensation. Shown are elastic collisions ("good" collisions) and the "bad" collisions due to background gas (for typical experimental conditions), elastic collisions, three-body recombination, and dipolar relaxation. (a) Atomic hydrogen; (b) sodium. For hydrogen, dipolar relaxation is the dominant source of bad collisions, whereas for sodium the dominant source is background gas collisions (at low densities) or three-body recombination (at high densities).

ping of the weak-field-seeking lower hyperfine state (which exists only for atoms with nuclear spin $I > \frac{1}{2}$). In this case, the energy release in dipolar relaxation approaches zero for small magnetic fields. This suppresses dipolar relaxation because of the centrifugal barrier in the exit channel (Tiesinga *et al.*, 1992) (or to state it more simply: for zero energy release, the process becomes elastic and has a vanishing rate at zero temperature). Note that reduction of G_{dip} would decrease T_* and thus decrease the lowest temperature achievable with evaporative cooling. In this sense, there is no fundamental limit for the lowest temperature achievable by

evaporative cooling. Some experiments have indeed magnetically trapped rubidium (Petrich *et al.*, 1995) and sodium (Davis *et al.*, 1995b) in the lower hyperfine state, but because this state was easily prepared rather than for the sake of suppressing dipolar relaxation.

Our experiment on sodium was the only alkali experiment that entered the region where inelastic collisions became important. At densities higher than 10^{14} cm^{-3}, the predicted trapping time due to three-body recombination is less than 1 sec (Moerdijk *et al.*, 1996a). The advantage of high density is the high speed of evaporation—the whole cooling process took only 7 sec. It appears that this experiment has already reached the maximum density at which evaporative cooling is still efficient.

Shlyapnikov *et al.* (1994) proposed another atom for evaporative cooling: spin polarized metastable helium (Fedichev *et al.*, 1996). The attractive feature of this system is a probably large "alkali-like" elastic collision cross section of 10^{-12} cm^2. Metastable helium has an additional loss process—Penning ionization, which severely limits the densities achievable in magneto-optical traps (Bardou *et al.*, 1992). However, this process is suppressed by five orders of magnitude in the spin polarized gas (Shlyapnikov *et al.*, 1994; Fedichev *et al.*, 1996). To obtain a sample of metastable helium with a high number of atoms and high density is still an experimental challenge, but efforts are under way (Rooijakkers *et al.*, 1995).

C. Enhanced Relaxation in the Condensate

Our discussion of collisions has focused on the situation before BEC occurs. Bose condensation in a trap is accompanied by a dramatic increase of the density, and as a result, by an increase of the rates for inelastic collisions. Due to Bose symmetry, the rate coefficients for dipolar relaxation and three-body recombination are smaller than for a normal gas, by factors of 2! and 3!, respectively (Kagan *et al.*, 1985; Hijmans *et al.*, 1993). Thus, the total loss rate for a pure condensate with density n is given by $G_{\mathrm{dip}}n/2 + Ln^2/6$.

The density increase during Bose condensation is limited by the repulsive interaction between the atoms. The mean field energy is given by $4\pi\hbar^2 na/m$, where a is the s-wave scattering length. At the BEC transition point with temperature T_c, the ratio r of thermal energy to mean field energy is $r = kT_c/(4\pi\hbar^2 n_c a/m)$, which is 50 for Na at 100 nK and 500 for hydrogen at 100 μK. This ratio r determines the maximum density increase of a condensate in a harmonic trap (assuming 100% condensate fraction): $n_0/n_c = 1.185r^{3/5}$, which is about 10 for Na and 50 for hydrogen.

In the recent BEC experiments on alkalis, condensate fractions close to 100% have been observed with lifetimes of 1 sec or more (Anderson *et al.*, 1995; Davis *et al.*, 1995b). A fully condensed sample of hydrogen will decay within 1 sec (Greytak, 1995). However, if evaporative cooling is slow, the increase of the inelastic collision rate might limit the buildup of the condensate fraction to a few percent (Hijmans *et al.*, 1993; Greytak, 1995).

D. Special Topics

In this section we want to briefly mention two more special aspects of evaporative cooling and refer to the relevant literature.

1. *Tuning the Cross Section*

The efficiency of evaporative cooling depends on the elastic collision cross section. The success of evaporative cooling in alkalis is mainly due to the large cross section for these systems. Usually, one regards the cross section as given and fixed by the choice of atom, but there are a few intriguing developments that might allow one to change or even tailor collisional properties.

One such development is the theoretical prediction that the scattering length for atoms in the lower hyperfine state can be tuned by an external magnetic field (Moerdijk *et al.*, 1995; Tiesinga *et al.*, 1992, 1993). This tuning exploits the fact that, for a hyperfine state that is not doubly polarized, there is a different hyperfine coupling for the separated atoms and the dimer. The difference in hyperfine and Zeeman interaction energies is used to vary the binding energy of the last bound state of the molecule and, therefore, the scattering length, which is uniquely determined by this binding energy.

However, large tuning will only be possible around so-called Feshbach resonances. No such resonance occurs for lithium and sodium in the range of magnetic fields where the lower hyperfine state is weak-field-seeking (Moerdijk *et al.*, 1995). For cesium and rubidium, the prospects of finding such a resonance at sufficiently low fields is larger, although the first experimental search was not successful (Newbury *et al.*, 1995).

Another way of changing collisional properties is by dressing atoms with radiofrequency, which can create resonances in collisions. Rf radiation might also increase inelastic collision rates. Fortunately, rf-induced exchange relaxation is negligible for the experimental parameters of rf-induced evaporation (Moerdijk *et al.*, 1996b).

Finally, the cross section of elastic collisions can be increased by optical shielding (see Heinzen, 1995, for a recent review). A blue-detuned laser

can be used to cause an avoided crossing between the potential curves of two colliding atoms. This creates a repulsive potential at large interatomic distances corresponding to a large value of the elastic cross section. The basic effect has been demonstrated by several groups (Sanchez-Villicana *et al.*, 1995; Walhout *et al.*, 1995; Marcassa *et al.*, 1994; Katori and Shimizu, 1994); however, it is not clear if adverse effects (heating, optical pumping) of the laser light can be avoided.

2. *Cooling Fermions*

So far, all efforts of evaporative cooling have concentrated on bosonic atoms. The major reason is their abundance in nature and ease of manipulation. In the quantum degeneracy regime at ultralow temperatures, fermions will show a behavior radically different from bosons. The only abundant alkali isotope that is fermionic is lithium-6. So far, only laser cooling of this isotope has been done. Deuterium, the fermionic hydrogen isotope, sticks much better than hydrogen to liquid helium–coated walls, and attempts to load deuterium in magnetic traps built for hydrogen were unsuccessful (Hijmans *et al.*, 1989; Doyle, 1996). Once fermions are successfully loaded, evaporative cooling would pose the challenge that elastic collisions can freeze out at very low temperatures (Koelman *et al.*, 1987). This is because s-wave collisions are forbidden for spin polarized fermions, and the cross section for p-wave collisions varies with temperature as T^2. For bosons, s-wave collisions dominate below temperatures of the order $\hbar^3/km^{3/2}C_6^{1/2}$, where C_6 is the coefficient characterizing the ground state van der Waals potential. For fermions, one might regard this temperature as an estimate for the temperature below which the elastic cross section freezes out. For alkalis, these temperatures are in the micro- to milli-Kelvin range and are easily reached by laser cooling. Further evaporative cooling of laser-cooled fermions is therefore not promising.

Several solutions can be envisioned. One is trapping of fermions in different hyperfine states. Fermions in different states would still undergo s-wave collisions. The trapping of different hyperfine states in an optical trap is straightforward, whereas in a magnetic trap, spin relaxation would limit the stability of the sample already at very low densities. It has been shown that this process can be sufficiently suppressed at bias fields of 10 T (Stoof *et al.*, 1996). Another route is to simultaneously trap two isotopes, where the thermalization happens through collisions between the different isotopes. The first experimental step toward such schemes has been done with the recent trapping of two isotopes in optical traps (Santos *et al.*, 1996; Süptitz *et al.*, 1994).

Finally, we want to mention that evaporative cooling is not limited to the atomic species mentioned in Section III.B. John Doyle at Harvard is planning such experiments with magnetically trapped molecules and other atomic species (Doyle *et al.*, 1995) (see Section IV.A.1).

IV. Experimental Techniques

A description of the experimental techniques for evaporative cooling is naturally divided in techniques for precooling (Section IV.A), trapping (Section IV.B), and evaporation (Section IV.E). The experimental efforts have developed along two rather separate lines, determined by the different properties of atomic hydrogen on the one hand, and the alkali-metal atoms on the other hand.

Nevertheless, there has been a substantial amount of cross-fertilization between the two fields: Magnetic trapping was first demonstrated for alkalis using laser cooling (Migdall *et al.*, 1985). Subsequently, it was used for hydrogen, in the first experiments on evaporative cooling (Hess *et al.*, 1987; Masuhara *et al.*, 1988; van Roijen *et al.*, 1988). Next, while work on laser cooling of alkalis developed toward high densities and long trapping times, bringing evaporative cooling in reach for the alkalis, optical cooling and detection techniques for hydrogen were developed (Luiten *et al.*, 1993; Setija *et al.*, 1993). The ultimate goal of evaporative cooling, reaching the quantum degenerate regime (Anderson *et al.*, 1995; Bradley *et al.*, 1995; Davis *et al.*, 1995b), was only achieved by a combination of techniques developed in once separated subfields.

A. Precooling

1. *Cryogenic Cooling*

The attainment of ultracold temperatures requires wall-free confinement; this is related to the fact that the lowest binding energy of any atom to walls is about 1 K, realized with hydrogen atoms and helium-coated walls. As a consequence, hydrogen cannot be cooled to below 75 mK in cells (Silvera, 1995a). The deepest traps that have been built with electromagnetic fields have a trap depth of about 1 K, thus requiring precooling of the atoms below this temperature as part of the loading process.

In the case of atomic hydrogen, there is a narrow temperature region in which hydrogen can already be magnetically trapped and where it does not stick to helium-covered walls. This technique was used at MIT (Hess *et al.*, 1987) and in Amsterdam (van Roijen *et al.*, 1988) to load magnetic traps.

Atomic hydrogen is generated in a low temperature rf discharge. The atoms migrate to the magnetic trapping region and thermalize with the helium-covered walls, resulting in a sample of magnetically trapped low-field seekers. Initially, both the c and d hyperfine states are present, but spin exchange collisions (predominately between the c-state atoms at these temperatures) lead to a doubly polarized sample of only d-state atoms within a few seconds.

Attempts with deuterium were unsuccessful so far, attributed to the 2.5 times larger binding energy of deuterium atoms with the walls (Hijmans *et al.*, 1989). Note that laser cooling, the method of choice for alkalis, is difficult for atomic hydrogen because of the prohibitively short wavelength (121.6 nm) of the 1s–2p transition; only one experiment with pulsed radiation has been reported (Setija *et al.*, 1993).

The idea of precooling by thermalization with a cryogenic environment was recently extended to a large class of paramagnetic atoms and molecules in a proposal by Doyle *et al.* (1995). Those species would stick to the cryogenic walls, but precooling can be achieved by a buffer gas of ^{3}He in the trapping region. The gas is kept at a temperature of 240 mK and a number density of 5×10^{15} cm^{-3}. This temperature is sufficiently low for magnetic confinement of the precooled particles. After the loading process, the ^{3}He is pumped out by lowering the cell temperature to 80 mK, thereby reducing the vapor pressure of ^{3}He to below 10^{-15} Torr. Subsequent evaporative cooling could then be used to reduce the temperature of the trapped gas.

A recently proposed scheme uses collisions to produce cold metastable helium (S. Yurgenson and J. A. Northby, personal communication, 1995). Helium atoms in a supersonic beam with a small velocity spread are excited to a metastable state by electron impact. The electron energy is chosen in such a way that the momentum transfer of the excitation process stops the helium atoms inside the trapping region of a magnetic trap.

2. *Laser Cooling*

Many atomic species can be cooled to submilli-Kelvin temperatures using laser cooling techniques. For evaporative cooling experiments, this has major advantages: (1) Precooling to temperatures around 100 μK allows much simpler construction of the magnetic trap using ordinary water-cooled conductors. (2) Atomic species can now be evaporatively cooled that have a much more favorable elastic collision cross section that atomic hydrogen. The ratio of good to bad collisions of alkali atoms can be 100 times higher than for hydrogen atoms (see Fig. 4). (3) The large elastic cross section of alkali atoms allows evaporative cooling times as short as several seconds,

which makes a cryogenic vacuum unnecessary (note that for hydrogen the cryogenic system was not only necessary for the excellent vacuum, but also for the superconducting magnets and the wall precooling). The major challenge for the laser coolers was to create laser-cooled samples with sufficiently long trapping times and high densities to start evaporative cooling.

The standard method for laser cooling begins with loading a magneto-optical trap (MOT) (Raab *et al.*, 1987) from a vapor cell (Monroe *et al.*, 1990; Cable *et al.*, 1990), or from a cold atomic beam cooled by either chirped slowing (Ertmer *et al.*, 1985) or Zeeman slowing (Phillips *et al.*, 1985). After switching off the weak magnetic field of the MOT, the temperature is lowered to approximately 10 recoil energies, by polarization gradient cooling (Lett *et al.*, 1989). Typically, this results in 10^7 to 10^{10} trapped atoms at densities of 10^{10} cm^{-3} to 10^{11} cm^{-3}. Higher densities of about 10^{12} cm^{-3} have been achieved in smaller clouds (Drewsen *et al.*, 1994; Townsend *et al.*, 1995). The temperature is limited by the recoil limit of polarization gradient cooling, whereas the density is limited by absorption and radiation trapping of the cooling light (Walker *et al.*, 1990) and by excited state collisions (Walker and Feng, 1994), and eventually also by level shifts due to the resonant dipole interaction (Castin *et al.*, 1995). The maximum phase space density achieved in this way is 10^{-4} to 10^{-5} (Drewsen *et al.*, 1994; Townsend *et al.*, 1995).

A major step forward was the development of the dark SPOT (Spontaneous Force Optical Trap) and dark polarization gradient cooling (Ketterle *et al.*, 1993). These techniques avoided the density limiting processes by keeping the atoms in a dark hyperfine state for most of the time. This allowed the confinement of more than 10^{10} atoms at densities of close to 10^{12} cm^{-3}. The dark SPOT technique closed the gap between the maximum densities usually achieved in laser cooling and the minimum densities required for evaporative cooling. This method was extended to rubidium (Anderson *et al.*, 1994) and cesium (Townsend *et al.*, 1996), and it was used in all realizations of evaporative cooling in alkali atoms (Adams *et al.*, 1995; Petrich *et al.*, 1995; Davis *et al.*, 1995a) with the exception of the Rice experiment, in which the lower density was compensated for by long cooling times (Bradley *et al.*, 1995).

Sub-recoil cooling techniques such as Raman cooling (Kasevich, 1995; Lee *et al.*, 1996; Kasevich and Chu, 1992; Davidson *et al.*, 1994; Reichel *et al.*, 1995), velocity-selective coherent population trapping (VSCPT) (Lawall *et al.*, 1994, 1995; Aspect *et al.*, 1988; Esslinger *et al.*, 1996), and adiabatic expansion of optical lattices (Kastberg *et al.*, 1995; Chen *et al.*, 1992) have been developed. These techniques might allow for even lower temperatures before loading the atoms into a magnetic trap, but this has yet to be

demonstrated experimentally. Only Raman cooling was used at densities larger than 10^{11} cm^{-3} (Kasevich, 1995; Lee *et al.*, 1996).

B. Conservative Traps

Evaporative cooling of atomic gases requires an environment for the atoms that insulates them from the "hot world." Any "thermal contact" with the cooled sample or any form of residual heating would require additional evaporative cooling and greatly reduce the cooling efficiency. Wall-free confinement of cold atoms provides excellent insulation. It can be achieved by various electromagnetic traps. Since evaporative cooling is used to cool below the recoil limit, none of the variants of the magneto-optical trap can be used. Conservative traps for neutral atoms have been realized mainly by two principles: static magnetic fields and far-off-resonant optical fields. The resource letter of Newbury and Wieman (1996) contains many references on atom traps.

1. *Magnetic Traps*

Maxwell's equations do not allow for a maximum of a static magnetic field in free space (Wing, 1984; Ketterle and Pritchard, 1992). Atoms are therefore trapped in the weak-field-seeking state at a minimum of the magnetic field. There are two classes of static magnetic traps (Bergeman *et al.*, 1987). In one case the minimum is a zero crossing of the magnetic field, characterized by the derivative B' of the magnetic field strength. The trapping potential is proportional to the absolute value of B, resulting in a linear, V-shaped potential. It is usually realized with the spherical-quadrupole field of two anti-Helmholtz coils. The other trapping topology has a parabolic minimum around a finite bias field. The parabolic trap was first suggested by Pritchard (1983) for atom trapping, and it is similar to the Ioffe configuration discussed earlier for plasma confinement by Gott *et al.* (1962). We refer to any configuration that is characterized by a nonzero bias field B_0 as an Ioffe–Pritchard (IP) trap. The lowest order expansion parameters for any $|B|_{\min} > 0$ trap are B_0, the axial field curvature B'', and the radial field gradient B' (Bergeman *et al.*, 1987). Several variants of this configuration have been discussed, such as the baseball trap or yin-yang trap. We regard them as alternative ways of winding coils to achieve the IP configuration, which in its most straightforward implementation consists of two pinch coils and four Ioffe bars (Bergeman *et al.*, 1987).

Bergeman *et al.* (1987) discuss the field geometry of an IP trap. The trap has two different regimes. For temperatures $kT < \mu B_0$ (where μ is the

atom's magnetic moment), the cloud experiences the potential of a 3D anisotropic harmonic oscillator with axial curvature $\mu B''$ and transverse curvature $\mu[(B'^2/B_0) - B''/2]$. In the case of $kT > \mu B_0$, the potential is predominantly linear along the radial direction (with a gradient of $\mu B'$) and harmonic along the axial direction. As a result, the δ parameter, characterizing the potential, changes from $\delta = \frac{3}{2}$ to $\delta = \frac{5}{2}$ for decreasing bias field. A low-bias-field IP trap is therefore advantageous for entering runaway evaporation. It features long cigar-shaped clouds. Such traps are in use in the hydrogen experiments at MIT (Greytak, 1995) and in Amsterdam (Walraven and Hijmans, 1994).

The efficiency and speed of evaporation are improved by strong confinement and adiabatic compression (see Section IV.D). Therefore, all groups pursuing evaporative cooling have developed tightly confining traps. In the hydrogen experiments this was achieved with superconducting magnets. Typical values in Amsterdam are $B'' = 440\ \mathrm{G/cm^2}$, $B' = 2 \times 10^4$ G/cm (Luiten, 1993). Only two groups in the alkali community have built superconducting magnetic traps: The historic experiment in Pritchard's group, which was the second magnetic atom trap ever built (Bagnato *et al.*, 1987), and a recent effort at Caltech (Willems and Libbrecht, 1995). Most alkali trappers try to avoid the added complexity of a cryogenic system; furthermore, in a cryostat the optical access to the trapping region would be limited.

Permanent magnets offer a simple alternative. The Rice group has combined efficient loading with tight field curvatures of about $1000\ \mathrm{G/cm^2}$ (Tollet *et al.*, 1995). Similar efforts were pursued by two groups in Germany (Ricci *et al.*, 1994; Frerichs *et al.*, 1992). An additional advantage compared with conventional magnets is the absence of noise on the trapping fields, which might otherwise cause heating. However, permanent magnets have the disadvantage that the magnetic fields cannot be changed or switched off, e.g., for adiabatic compression or time of flight diagnostics.

The linear trap offers superior confinement compared with a parabolic trap. This follows from the simple argument that coils that are a distance R_{coil} away from the trapped cloud and generate a field B_{coil} at the coil, produce a field gradient of $B' \approx B_{\mathrm{coil}}/R_{\mathrm{coil}}$ and a curvature of $B'' \approx B_{\mathrm{coil}}/R_{\mathrm{coil}}^2$. A cloud of size r in a linear potential with gradient B' would be confined to the same size by a curvature that is equal to B'/r. The "effective curvature" of linear confinement is therefore $B_{\mathrm{coil}}/rR_{\mathrm{coil}}$. This exceeds the curvature of a parabolic trap by R_{coil}/r, which is usually an order of magnitude or more.

A linear potential was used for the first magnitude trap (Migdall *et al.*, 1985). When it was employed for the first demonstrations of evaporative cooling with alkali atoms (Davis *et al.*, 1994; Petrich *et al.*, 1994b), trap loss

due to Majorana flops (Schwinger, 1937; Migdall *et al.*, 1985; Phillips *et al.*, 1985; Bergeman *et al.*, 1989) near the zero of the magnetic field was encountered. These spin-flips to the high-field-seeking state occur due to a violation of the adiabatic condition that requires the Larmor frequency to be larger than the angular frequency at which the moving atoms perceive a rotating magnetic field. This region of low magnetic field has a size of about $\sqrt{2\hbar v/\pi\mu B'}$, which is about 1 μm for a velocity $v = 1$ m/sec and $B' = 1000$ G/cm, and was dubbed "the hole in the trap." As long as the hole is small compared with the cloud diameter, the trapping time is long (even longer than a minute) and evaporative cooling can increase the phase-space density by more than two orders of magnitude (Davis *et al.*, 1995a). However, as the temperature drops, the trap loss due to the hole becomes prohibitive for further cooling.

Two methods have been demonstrated to plug the hole. One solution is to add a rotating magnetic field to the anti-Helmholtz trap. The rotating frequency is much higher than the orbiting frequency of the atoms, and much lower than the Larmor frequency. The resulting time-averaged, orbiting potential (TOP) trap is harmonic, but much tighter than what could be obtained by dc magnets of the same size (Petrich *et al.*, 1995) (see *Note added in proof*). Typical field curvatures in the TOP trap are B'^2/B_{rot}, where B_{rot} is the (constant) magnitude of the rotating field (about 10 G).

Another solution is to plug the hole by using electric dipole forces from a tightly focused blue-detuned laser beam (see also Section IV.B.2), which repels atoms from the center of the trap (optically plugged magnetic trap) (Davis *et al.*, 1995b). The optically plugged trap achieved very tight confinement corresponding to a curvature of about B'/x_0, where x_0, the separation of the potential minimum from the zero of the magnetic field, was about 50 μm. The geometric average of the three curvatures exceeded the value for the TOP trap by a factor of 12. The disadvantage is the need for precision (micrometer) alignment of the laser beam with respect to the trap center.

To summarize, sufficiently tight confinement in a magnetic trap has so far only been achieved with one of the following experimental "nuisances": superconducting coils, permanent magnets, rotating magnetic fields, or the optical plug (see *Note added in proof*).

2. *Optical Traps*

Optical dipole traps (Chu *et al.*, 1986) rely on the principle that an off-resonant laser beam attracts or repels atoms, depending on whether it is red- or blue-detuned. The trap depth depends on the laser intensity divided by the detuning, whereas the spontaneous rate of light scattering scales as the intensity divided by the square of the detuning, i.e., as the

trap depth divided by the detuning. Heating due to spontaneous scattering can therefore be avoided if intense, far-detuned laser light is used (Phillips, 1992; Miller *et al.*, 1993).

The only evaporative cooling experiment in a dipole trap was performed at Stanford by Adams *et al.* (1995). The trap consisted of two crossed red-detuned Nd:YAG laser beams (1.06 μm) far detuned from the 589-nm sodium resonance. Up to 8 W of total power in the two beams provided up to 900 μK trapping potential with an estimated heating rate of 1 photon/sec or 0.5 μK/sec. Such a heating rate requires fast evaporative cooling, which is possible due to the high atomic densities in dipole traps. The heating should be negligible if a CO_2 laser at 10.6 μm is used. Such a quasi-electrostatic trap has been demonstrated by Takekoshi and Knize (1996).

If only a single beam is used, the dipole trap has weak confinement along the axial direction. A recently demonstrated electro-optical hybrid trap used electrostatic confinement along the axial direction by surrounding the beam waist with a high voltage electrode (Lemonde *et al.*, 1996).

A blue-detuned dipole trap has the advantage that atoms are repelled by the laser beams and trapped in the dark; this greatly reduces residual spontaneous scattering and, therefore, the heating rate. In such a trap, the atoms are surrounded by repulsive walls of blue-detuned light. Gravity can replace one of the walls. Such a trap was demonstrated by Davidson *et al.* (1995). A very flexible trap geometry can be achieved by rotating a laser beam with an acousto-optical modulator (Thompson *et al.*, 1995). Larger trapping volumes can be realized within an enhancement cavity (Han *et al.*, 1995). Another related trapping geometry is an atom cavity employing evanescent-wave mirrors and gravity for confinement (Aminoff *et al.*, 1993).

A problem needing further study is heating due to beam jitter, especially if more than one laser beam is used to form the trapping potential. In comparison with magnetic traps, optical traps have the advantage that the trapping potential can be switched in less than 1 μsec, whereas magnetic traps have typical (inductive) time constants of 1 msec. Furthermore, some precision experiments (e.g., search for an electron electric-dipole moment (EDM), frequency standards) require the absence of inhomogeneous magnetic fields. Blue-defined traps are harder to load than red-detuned traps because they are missing the "sucking" action of red-detuned light.

An interesting future direction could be a hybrid approach using dipole and magnetic forces. A first realization of his concept was the optically plugged magnetic trap (Davis *et al.*, 1995b), but one can envision further variants such as a red-detuned laser focused into a magnetic trap. The magnetic field would act as an enormous funnel to collect atoms and

evaporatively cool them into the "deep dimple" of the potential created by the optical dipole force. Another possibility is to generate a Bose condensate in a magnetic trap and then (adiabatically or suddenly) transfer the atoms into some form of dipole trap—maybe by rotating a blue-detuned laser beam around the atoms similar to the trap just mentioned above (Thompson *et al.*, 1995). In any case, dipole forces can by applied with extremely high spatial and time resolution, and we expect them to play an important role in experiments with evaporatively cooled atoms.

3. *Special Traps*

The limit for evaporative cooling of hydrogen in a conventional magnetic trap is dipolar relaxation. This is avoided if atomic hydrogen can be trapped in the ground hyperfine state (the *a* state). This can be achieved in a microwave trap (Agosta *et al.*, 1989), which is the magnetic dipole analog of the electric-dipole-force laser trap mentioned in the previous section. The ultimate goal is to combine such a trap with a conventional magnetic trap as a hybrid trap (Silvera and Reynolds, 1991; Silvera, 1995b). Since the trap depth of the microwave trap is only on the order of several milli-Kelvin, hydrogen would be first trapped in the *d* state, evaporatively cooled to a few hundred micro-Kelvin, then transferred into the microwave trap, and further cooled by evaporation.

A microwave trap was recently demonstrated with laser-cooled cesium (Spreeuw *et al.*, 1994). This trap was only 0.1 mK deep, mainly due to the strong influence of gravity on Cs. The gravitational pull on the Cs atoms was compensated for by a magnetic field gradient, which affected the trapping strength significantly (due to the resulting gradient in the detuning of the microwave field). For hydrogen, the situation would be much better.

Another way to trap strong-field-seeking atoms is an ac magnetic trap. It was suggested in 1985 for atomic hydrogen (Lovelace *et al.*, 1985), and realized in 1991 with Cs (Cornell *et al.*, 1991). This trap is much weaker than dc magnetic traps, and it has not been pursued beyond the first demonstration. Finally, ac electric fields offer another possibility to trap strong-field seekers (Riis and Barnett, 1993; Shimizu and Morinaga, 1992). However, the forces are very weak unless extremely small separations between the electrodes are chosen.

C. Laser Cooling inside Conservative Traps

Laser cooling the atoms after they have been loaded into a conservative trap has a double advantage: As the temperature is reduced, the density increases proportional to $T^{-\delta}$, resulting in an increase in phase space of

$T^{-\delta-3/2}$ without loss in the number. However, this is only possible until limitations of laser cooling are reached, which are due to absorption of the cooling light or to inelastic collisions.

So far, Doppler cooling inside a magnetic trap has been demonstrated by Pritchard's group at MIT for sodium (Helmerson *et al.*, 1992b), by the Rice group for lithium (Tollet *et al.*, 1995), and by the Amsterdam group for hydrogen (Setija *et al.*, 1993). In all these experiments, the atoms were loaded directly into a magnetic trap, not transferred from another trap (e.g, a MOT). Atoms released from a MOT are usually already cooled to or below the ultimate temperature of Doppler cooling, and cooling after the transfer would only compensate for the temperature increase during the transfer—which is usually only a small factor.

The gain in phase-space density is larger when sub-Doppler or even sub-recoil schemes are employed. The group in Boulder has recently cooled magnetically trapped atoms with gravitational Sisyphus cooling; this cooling scheme involves both rf transitions and optical pumping in such a way that the atom experiences a steeper potential when moving outward from the trap center than when moving inward (Newbury *et al.*, 1994). This scheme realized the earlier proposal of Pritchard (1983) and Pritchard and Ketterle (1992), then called cyclic cooling.

Raman cooling down to the recoil limit was applied to sodium atoms in an optical dipole trap, resulting in a final density of 4×10^{11} cm^{-3} and temperature of 1.0 μK (Lee *et al.*, 1996), the highest phase-space density which has been achieved so far by optical cooling. The limitation was probably related to inelastic hyperfine changing collisions.

Cyclic cooling can in principle reach sub-recoil temperatures. However, the schemes which have reached sub-recoil temperatures thus far are not compatible with magnetic trapping, but they are compatible (at least in principle) with optical dipole traps (Dum *et al.*, 1994; Pellizzari and Ritsch, 1995). With the recent progress in Raman cooling (Lee *et al.*, 1996; Reichel *et al.*, 1995) and velocity-selective coherent population trapping (Lawall *et al.*, 1995; Esslinger *et al.*, 1996), there is hope to reach extremely high phase-space densities in far-off-resonant dipole traps, requiring only a modest step of evaporative cooling to reach quantum degeneracy.

D. Adiabatic Compression

Adiabatic compression is a simple technique, but we want to emphasize the importance of such a compression of the atom cloud prior to evaporative cooling. If, after the loading, the potential is adiabatically increased by a factor a, the temperature rises by a factor $a^{2\delta/(2\delta+3)}$ and the density by $a^{3\delta/(2\delta+3)}$. Phase-space density is, of course, constant, but the elastic collision rate and, therefore, the speed of evaporative cooling has been

increased by a factor $a^{4\delta/(2\delta+3)}$. The ratio of good to bad collisions goes up, either in proportion to the speed (when background gas collisions are the dominant loss mechanism) or in proportion to $\sqrt{T}$ in the case of dipolar relaxation. In the evaporative cooling experiments in Boulder and by our group, adiabatic compression was essential. Davis *et al.* (1995a) increased the collision rate by a factor of 20 by this technique. Generally, it is always favorable to work at the tightest confinement until three-body recombination sets in or the sample becomes collisionally thick. Those limits were reached in the MIT sodium experiment (Davis *et al.*, 1995b). In hydrogen experiments, the density to reach collisional thickness is relatively low because the sample is cigar-shaped and the evaporation is one-dimensional along the long axis (see Section IV.E.3). In these experiments, the dense regime is avoided by lowering the radial confinement (Graytak, 1995; Doyle *et al.*, 1994).

E. Evaporation Techniques

Evaporative cooling is most efficient if the high energy atoms, produced in collisions, leave the trap without experiencing additional collisions. All techniques of evaporation select the most energetic particles spatially; i.e., it is a selection based on potential energy. It is conceivable to perform the selection based on velocity using the Doppler shift of a narrow resonance line and thus select particles according to their kinetic energy, but since the kinetic and potential energy distributions are related by the virial theorem, there is no obvious advantage in velocity selection. The different evaporation techniques to be discussed here differ in the manner of spatial selection. As will be discussed, the evaporation mechanism and the trap geometry play important roles in the efficiency of the cooling.

1. *Direct Contact with Walls*

The simplest conceivable scheme for evaporation is to have a sticky wall close to the atom cloud, which absorbs the high energy tail of the distribution. Such a method was already used in the first realization of electromagnetic confinement of neutral particles, the neutron storage ring by Paul and collaborators (Kügler *et al.*, 1985). A movable beam scraper was used to remove neutrons on outer orbits. Absorption to the walls provided the initial evaporative cooling in the MIT hydrogen experiment (Hess *et al.*, 1987). During the loading, the walls are kept at a higher temperature (about 250 mK), at which the desorption rate is higher than the rate of surface recombination. Subsequently, the wall temperature is

lowered, and it acts as an absorbing surface providing evaporative cooling. As the cloud shrinks, the evaporation process slows down, and it is subsequently forced by ramping down the axial trap depth (to be discussed) or by moving the sample closer to the walls (D. G. Fried, personal communication, 1996).

In Amsterdam, the surface was kept at a constant temperature of 200 mK, and the evaporation was triggered by boiling off the helium film from the surface of a bolometer, thus creating a sticky surface for atomic hydrogen (where the atoms recombine) (Luiten *et al.*, 1993). Various aspects of whether a wall is sticky (i.e., it removes atoms) or provides thermalization are exhaustively discussed by Setija (1995).

Evaporation to the walls is initially a two- (or even three-) dimensional process, depending on the geometry of the cell. Forcing evaporation by moving the sample toward one wall may result in 1D evaporation, which is much less effective.

2. *Lowering the Total Trapping Potential*

Evaporative cooling can be forced by lowering the total trapping potential. This was done in the crossed dipole trap in Stanford, wherein the total laser power was ramped down (Adams *et al.*, 1995). This is essentially an adiabatic decompression; however, after decompression there are fewer bound states in the potential, and evaporation occurs because states that were bound in the tight potential correspond to continuum states after decompression. The method is very simple, but it has the major disadvantage that the collision rate becomes very small during the decompression. One might have to repeat several compression/decompression cycles, where intermediate compression speeds up the thermalization. A potential disadvantage of this repetitive scheme is that the cold atoms are not left alone; rather, they are continuously compressed and decompressed. Unless this is done fully adiabatically, some heating might occur.

3. *Saddle Point of the Potential*

The disadvantage of the previous method is due to the proportionality between trap depth and confinement. This was avoided in the MIT hydrogen experiments, where evaporation was forced by lowering only the axial trapping potential (Masuhara *et al.*, 1988; Hess, 1986). The hottest atoms escaped over the saddle point along the axial direction. The trapping volume, and therefore the collision rate, could be controlled independently through the radial potential. This decoupling between confinement and trap depth allowed continuous evaporation. Eventually, when the

mean free path became comparable with the axial length of the sample, the radial confinement was lowered to avoid collision times shorter than the axial oscillation period.

The saddle-point method is a 1D selection method because it selects the atoms due to their axial energy. If the ergodic mixing time is longer than the time between elastic collisions, this decreases both the speed and efficiency of evaporation (Surkov *et al.*, 1994, 1996). In some of the MIT experiments on hydrogen ergodic mixing was fast enough to ensure 3D evaporation (Doyle, 1996).

4. *Radiative Evaporation*

Pritchard and collaborators were the first to perform rf spectroscopy of magnetically trapped atoms. They used the rf lineshape to determine the energy distribution of the trapped atoms (Martin *et al.*, 1988; Helmerson *et al.*, 1992a). In 1989, they suggested that this method could be used to perform evaporative cooling. More generally, they introduced the concept of *radiative evaporation*, which means that a radiation field is used to transfer atoms from a trapped to an untrapped state in an energy-selective way (Pritchard *et al.*, 1989). There are two ways of implementing this concept: (1) narrow rf or optical transitions, which are energy-selective due to the one-to-one correspondence between Zeeman shift and potential energy in a magnetic trap, or (2) a laser beam focused to the edge of a large cloud, which causes spatially selective optical pumping to an untrapped state. In the latter case, the linewidth of the transition may be broad.

The Amsterdam group independently suggested the concept of spatially selective microwave or optical transitions, and they proposed an additional way of spatial selection: A near-resonant laser beam would be absorbed in the outer layer of the cloud and automatically perform spatially selective optical pumping (Hijmans *et al.*, 1989). The cold atoms are shielded by the more energetic atoms and are unaffected. This method, called light-induced evaporation, was demonstrated in a proof-of-principle experiment in Amsterdam by Setija *et al.* (1993).

The most successful implementation of radiative evaporation in rf-induced evaporation. The original suggestion (Pritchard *et al.*, 1989) mentioned three advantages compared with the saddle-point method: (1) The magnetic trapping potential does not have to be modified for the evaporation and can thus be kept at the optimum confinement. (2) The escape rate and the potential energy of the escaping atoms is easily controlled by the amplitude and frequency of the applied radiation. (3) The space where the

particles escape from the trap is given by the shell where the rf transition is tuned into resonance by the local magnetic field, and thus it is not limited to a saddle point in the trapping potential.

The use of rf-induced evaporation was first reported at the 1993 OSA meeting (Ketterle *et al.*, 1993). Most of the evaporative cooling experiments on alkalis used this technique, as will be discussed in Section V.B. In the following, we discuss two aspects of rf-induced evaporation in more depth: the process of evaporation in the adiabatic and diabatic limits and the dimension of the rf-induced evaporation for different traps.

Adiabatic and Diabatic limit of Rf-induced Evaporation. Rf-induced evaporation can be described in the dressed-atom formalism (Cohen-Tannoudji *et al.*, 1992), where the different m_F states of an atom with spin F are coupled to an rf field, which we assume to be linearly polarized: $\vec{B}_{\rm rf}(t) = B_0 \cos(\omega t)\hat{e}_{\rm rf}$.

The coupling matrix element between levels $|F, m_F\rangle$ and $|F, m_F \pm 1\rangle$ is $(1/4)g\mu_B B_0(\hat{e}_{\rm rf} \times \hat{e}_z)\sqrt{F(F+1) - m_F(m_F \pm 1)}$, where g is the atomic g factor, and the trapping field points along the quantization axis $\hat{e}_z$.

The adiabatic potential curves $U(r)$ are obtained by finding the dressed-state eigenvalues for the local magnetic field $B(r)$. In the dressed-atom picture, one considers the total energy of the atom plus the field of N rf photons. Without coupling, this simply means that $N\hbar\omega$ is added to the atomic Zeeman energies, resulting in a Zeeman pattern for each N that is vertically displaced by $N\hbar\omega$. At positions where the rf field is in resonance, curves with $\Delta N = 1$ cross. The coupling transforms these crossings into avoided crossings. This determines the pattern of the adibatic energy levels (Fig. 5b).

A slowly moving atom stays on the adiabatic potential curve. As an example, we assume that an atom in the $|F, F\rangle$ hyperfine state moves outward from the center of the trap. When it comes close to resonance, the rf field mixes this state with the other m_F states, which leads to a flatter potential curve. Beyond the resonance point, the atomic state has been adiabatically transformed into a nontrapped, strong-field-seeking state, and the atom is repelled from the trap. While traversing the avoided crossing, the atom has thus emitted $2F$ rf photons in a stimulated way and reversed the direction of both electron and nuclear spin.

This picture of rf-induced evaporation emphazises the similarity with other evaporation methods because the radiofrequency leads to an adiabatic potential surface with a trap depth that is approximately $|m_F|\,\hbar(\omega - \omega_0)$, where ω_0 is the rf resonance frequency in the center of the trap. The evaporation process is then just the "spilling" of the most energetic atoms out of the trap.

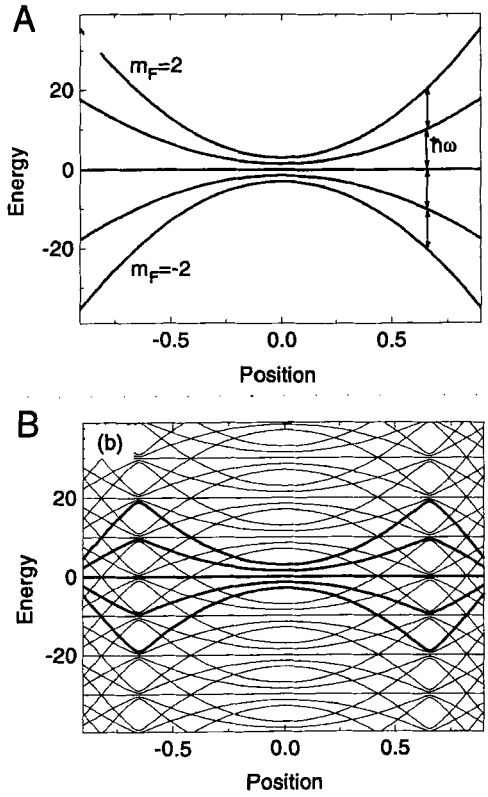

FIG. 5. Potential curves for rf-induced evaporation of an atom with spin $F = 2$, in a quadratic trap with nonzero bias field. (a) Diabatic curves, for different m_F sublevels, relevant for weak rf fields. The arrows indicate the position where the rf, with frequency ω, is resonant. (b) Adiabatic curves (dressed-atom energy levels), relevant for strong rf fields. The pattern is periodic in energy, with spacing $\hbar\omega$. One set of curves is drawn with fat lines, to show how trapped states adiabatically evolve into untrapped states, and vice versa, around the resonance position.

This adibatic picture is valid as long as an adiabaticity condition is fulfilled. This condition requires that the energy gap due to the avoided crossing be larger than the energy uncertainty related to the finite amount of time that an atom with velocity v spends in the region of resonance. For a two-level system coupled by a matrix element V_{12}, and an atom moving with velocity v along the x axis, the transition probability P between the adiabatic curves is given by the Landau–Zener formula (Rubbmark *et al.*,

1981) $P = 1 - \exp(-\xi)$, with $\xi = 2\pi |V_{12}|^2/\hbar g \mu_B B' v$. The Landau–Zener theory is strictly valid only for a two-level system, and we use it here only for a qualitative discussion of the two limiting cases.

For a weak rf field, $\xi \ll 1$, P is much smaller than unity; i.e., the atoms predominately stay on the diabatic surface shown in Fig. 5(a). The transition probability for a spin-flip is $P \approx \xi$, which describes the diabatic limit of rf-induced evaporative cooling: The atomic energy levels are almost unperturbed, the atoms slosh many times through the resonance shell, and only after $1/P$ oscillations are they spin-flipped from the $|F, F\rangle$ to the $|F, F-1\rangle$ hyperfine state.

The adiabatic limit is clearly the ideal situation for evaporative cooling. However, the evaporation process in a trap (with oscillation time T_{osc}) saturates at a lower rf power. The condition for saturation is $P \approx T_{\text{osc}}/\tau_{\text{el}}$, which means that an energetic atom evaporates before it collides again. In the case of $F > 1$, we have the additional complication that an atom that has been spin-flipped from the $|F, F\rangle$ state to the $|F, F-1\rangle$ state is still trapped (see Fig. 5) and can undergo spin exchange collisions with the trapped atoms, leading to heating and trap loss. The evaporating atom reaches an untrapped state after losing $F\hbar$ of spin angular momentum which due to the randomness of spin-flips up and down requires a time of $F^2 T_{\text{osc}}/P$. This has to be shorter than the spin exchange time $\tau_{\text{ex}} \approx 1/G_{\text{ex}} n_0$. To achieve the full efficiency of evaporation, the probability P for spin-flips thus has to satisfy

$$P > T_{\text{osc}} \left(\frac{1}{\tau_{\text{el}}} + \frac{F^2}{\tau_{\text{ex}}} \right) \tag{16}$$

With a typical rate coefficient for spin relaxation of $G_{\text{ex}} \approx 10^{-12}$ cm^3/sec and an elastic cross section of 10^{-12} cm^2, the second term is dominant for velocities smaller than a few centimeters per second.

Only the magnetic field component of the rf *perpendicular* to the magnetic trapping field induces spinflips. The directions of the trapping field on the surface for evaporation cover the full solid angle in certain traps, e.g., in the spherical quadrupole trap and in an IP trap with small bias field. As a result, there are two points where the transition matrix elements are zero, because the trapping field and the rf field are parallel. In an area around these points, the diabatic coupling case is realized. In practice, the rf transition can be sufficiently saturated so that this area is small and does not strongly affect the speed of evaporation.

Dimension of Rf-Induced Evaporation. Rf-induced evaporation spin-flips atoms on a resonant shell where $g \mu_B B = \hbar \omega_{\text{rf}}$. This shell surrounds the

trapped atoms. Rf-induced evaporation is a 3D evaporation technique if shells with $|B| = \text{const}$ are equipotential surfaces. This is the case in a dc magnetic trap, as long as gravity can be neglected.

However, gravity pulls the cloud downward in the magnetic potential; the bottom of the cloud experiences higher magnetic field. Since evaporating atoms have an average excess energy of κkT with $\kappa \approx 1$, evaporation happens mainly at the bottom when the gravitational energy varies by more than $\pm kT$ over the equipotential surface $U = \eta kT$. For harmonic confinement along the z axis, $U = U'' z^2/2$, this equipotential surface is at $z \approx \sqrt{2\eta kT/U''}$. Evaporative cooling becomes one-dimensional for

$$kT < \frac{2\eta(mg)^2}{U''} \tag{17}$$

To express this condition in more practical units, we denote by $B'_{\text{grav}} = mg/\mu$ the magnetic field gradient that counterbalances gravity (e.g. 4.1 G/cm for Na in the $|2,2\rangle$ hyperfine state). With the magnetic field curvature B'' along the z axis, Eq. (17) is equivalent to

$$kT < \frac{2\eta\mu B'^2_{\text{grav}}}{B''} \tag{18}$$

For $B'' = 500$ G/cm^2 and $\eta = 5$, the limiting temperature is 1 μK for ^{7}Li, 10 μK for Na, and 150 μK for Rb. Below this temperature, evaporative cooling becomes less efficient. In the Li experiment at Rice (Bradley *et al.*, 1995), this only happens at temperatures close to the onset of quantum degeneracy. The MIT Na experiment operated at a vertical field curvature of $\approx 5 \times 10^4$ G/cm^2, which was high enough to avoid 1D evaporation (Davis *et al.*, 1995b). One-dimensional evaporation will affect the cooling most strongly for small ratios of good to bad collisions. One-dimensional evaporation might be unavoidable because a sufficiently large B'' cannot be provided for the lowest desired temperature. In this case, the experimental strategy should be to speed up evaporation in the first phase and obtain a large value for R, so that evaporation does not fall below the threshold for runaway evaporation when λ increases due to the onset of 1D evaporation (see Eq. (7)).

For a linear potential characterized by a field gradient B', the criterion for 1D evaporation is

$$B' > \eta B'_{\text{grav}} \tag{19}$$

which is independent of temperature. In the adiabatic potential picture, 1D evaporation can be visualized as a volcano crater with a slanted rim

due to gravity. Atoms spill out at the lowest part of the rim, which is now a saddle point of the total adiabatic potential.

The geometry of evaporation is very different in the TOP trap (see Section IV.B.1). The surface for evaporation is always the portion of the outer shell of the cloud that is exposed to the highest magnetic field. In the TOP trap the magnetic field varies periodically, and the shell for evaporation are the points $\vec{r}$, where $\max_t |B(\vec{r}, t)| = \hbar \omega_{\mathrm{rf}}/g \mu_B$ and the maximum is taken over one period of the rotating field (Fig. 6). This shell is approximately a cylinder, or more precisely a barrel, but the curvature is negligible. For a rotating horizontal bias field, gravity displaces the cloud only along the cylinder axis, and evaporation is always 2D. If the bias field rotates in a different way, the cylinder is tilted with respect to the vertical axis, and a displacement of the cloud by gravity leads to 1D evaporation. The critical displacement is about $1/\sqrt{8\eta}$ of the cloud diameter.

The major step toward evaporative cooling in alkalis was the attainment of a sufficiently large ratio of good to bad collisions for runaway evaporation. Our theoretical discussion in Section IV.D suggests that this ratio might be an order of magnitude larger for 1D evaporation. The three successful BEC experiments avoided 1D evaporation because of three different reasons: the magnetic field rotating around a vertical axis for Rb (Anderson *et al.*, 1995), the light mass of Li (Bradley *et al.*, 1995), and the tight confinement for Na (Davis *et al.*, 1995b). However, the important question of the dimension of evaporation was first addressed in detail by

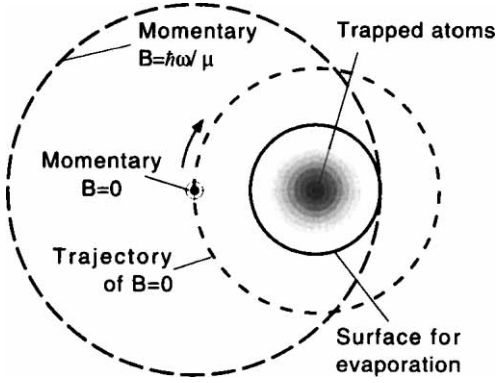

FIG. 6. The geometry of rf-induced evaporation in the TOP trap. Shown here is the plane through the trap center and the rotating bias field.

Surkov *et al.* (1996), so that probably these three solutions were found without really knowing the problem!

5. *Other Schemes*

There are other possible methods for evaporating atoms. Every loss process that happens predominately for atoms in the outer part of the cloud has a cooling effect. In the TOP trap, the rotating zero of the magnetic field leads to Majorana flops and was used for the initial cooling of the cloud (Petrich *et al.*, 1995). Similarly, in the optically plugged trap (Davis *et al.*, 1996b), the plug was initially "submerged" by the initial atom cloud, which might have resulted in some additional cooling due to Majorana flops. However, in both cases the evaporation is of lower dimension and is probably inferior to rf-induced evaporation.

6. *Relation to Other Cooling Methods*

Evaporative cooling relies on selective removal of energetic atoms and on elastic collisions. Another cooling scheme that relies on collisions is sympathetic cooling: One species is cooled by collisional thermalization with another species that is kept at a cold temperature. So far, this scheme has only been realized with trapped ions (Larson *et al.*, 1986; Imajo *et al.*, 1996).

The selection of energetic atoms is of course also an important part of many optical cooling schemes. In Raman cooling (Kasevich and Chu, 1992), velocity-selective coherent population trapping (VSCPT) (Aspect *et al.*, 1988), and cyclic cooling (Pritchard, 1983; Newbury *et al.*, 1994; Cirac and Lewenstein, 1995) [which are examples of phase-space optical pumping (Pritchard *et al.*, 1987)], energetic atoms are selectively excited using narrow optical or rf resonances. However, in contrast to evaporative cooling, these atoms are cooled and recycled. The success of evaporative cooling demonstrates that it is much easier to select atoms and waste them than to cool them!

There is one cooling method that relies on the absence of collisions: one-dimensional adiabatic cooling, which has been discussed for obtaining antihydrogen below 1 mK (Shlyapnikov *et al.*, 1993). In this case, the goal is to avoid the mixing with the motion in the other two dimensions to get the maximum cooling effect in the vertical dimension. That is just the opposite of what is desirable in evaporative cooling, but studies of ergodic behavior of trapped atoms are relevant for both adiabatic and evaporative cooling (Surkov *et al.*, 1994, 1996).

V. Summary of Evaporative Cooling Experiments

Evaporative cooling of atomic gases has so far only been demonstrated by a limited number (six) of groups. In this section, we give an overview and a comparison of the evaporative cooling experiments reported so far. Although the number of experiments is limited, and most of them were demonstration experiments rather than careful studies and optimizations of evaporative cooling, we feel that the tabular comparison of the speed and efficiency of the cooling provides insight.

A. Hydrogen

Evaporative cooling of an atomic gas was first observed by the Greytak/Kleppner group (Hess *et al.*, 1987). The temperature of the gas was estimated to be 40 mK from the long lifetime of the trapped atoms, consistent with evaporative cooling by adsorption and recombination on the walls of the cell. Because of the limited diagnostics (only the number of trapped atoms could be measured by nuclear spin resonance), little information about the evaporation process could be gained.

This group proceeded in the next year to forced evaporative cooling (Masuhara *et al.*, 1988). As the atoms (evaporatively) cooled, the axial depth of the trapping potential was lowered exponentially, while the radial confinement was simultaneously reduced. The radial trap depth was always kept larger than the axial depth, resulting in evaporation over a saddle point of the potential. A considerable increase in phase-space density was observed. Much more information could be extracted by a more sophisticated detection scheme (Doyle *et al.*, 1989). With a bolometric detection technique, and by quickly ramping down the trapping rim, the energy distribution of the trapped particles was measured. Temperatures as low as 800 μK were reported in 1989.

The closest approach to BEC of hydrogen to date was made in 1991 (Doyle, 1991; Doyle *et al.*, 1991) when densities as high as 8×10^{13} cm^{-3} and temperatures as low as 100 μK were reported. Further progress was impeded by the limits of the bolometric detection method. The sticking probability of hydrogen on the superfluid ^{4}He surface was measured at submilli-Kelvin temperatures, and quantum reflection was demonstrated. The evaporative cooling process was in good agreement with model calculations.

Very recently, trapped atomic hydrogen was observed by two-photon spectroscopy (Cesar *et al.*, 1996). This provided not only greatly improved

sensitivity, but also nondestructive monitoring of the cooling process, and should result in further improvement of the evaporative cooling.

In Amsterdam, magnetic trapping of hydrogen was reported in 1988 (van Roijen *et al.*, 1988). In 1993, using Lyman α spectroscopy, an accurate comparison of the cooling process with a theoretical model was made (Luiten *et al.*, 1993, 1994). These experiments were performed in a fixed field geometry, and the evaporation process was suddenly switched on by boiling off the helium coating on a bolometer, thus creating a sticky surface for hydrogen atoms.

In the same year, this group succeeded in demonstrating Doppler cooling for hydrogen, the first laser cooling experiment with hydrogen. This allowed them to reach significantly higher initial phase-space densities before evaporative cooling. Furthermore, light-induced evaporation was demonstrated (Setija *et al.*, 1993).

B. Alkali Atoms

The achievement of evaporative cooling of alkali atoms was announced by the MIT and JILA groups at IQEC in May 1994 and reported at ICAP-14 (Davis *et al.*, 1994; Petrich *et al.*, 1994b). In the same summer, the Stanford groups also observed evaporative cooling, in an optical trap (Lee *et al.*, 1995). The results appeared in referred journals in the first half of 1995 (Adams *et al.*, 1995; Davis *et al.*, 1995a; Petrich *et al.*, 1995), and by the end of 1995, two of these groups had reported the observation of BEC (Anderson *et al.*, 1995; Davis *et al.*, 1995b), while a fourth group had observed evaporative cooling of alkalis and also obtained evidence for BEC (Bradley *et al.*, 1995).

In the JILA experiment, a dark SPOT trap was loaded from a room temperature vapor cell at 10^{-11} Torr (Anderson *et al.*, 1994). The low pressure was needed to achieve long trapping times, but it slowed down the loading process to 5 min. Approximately 10^6 atoms were trapped. A magneto-optic compression scheme (Petrich *et al.*, 1994a), polarization gradient cooling, and optical pumping were applied before suddenly switching on the TOP trap, and starting rf-induced evaporation (Anderson *et al.*, 1995).

In the MIT sodium experiments, a thermal beam of sodium atoms was slowed in a Zeeman slower (Joffe *et al.*, 1993) and trapped in a dark SPOT trap (Ketterle *et al.*, 1993). This technique yielded large numbers of atoms ($\approx 10^{10}$) at high densities (5×10^{11} cm^{-3}), within a 2-sec loading time. After polarization gradient cooling, a spherical-quadrupole trap was suddenly switched on, and rf-induced evaporation was performed. Majorana flops were prevented by an optical plug (Davis *et al.*, 1995b).

In the Stanford experiment, a crossed-dipole trap was loaded from a magneto-optical trap. In the final stage of the loading, the (temporal) dark SPOT technique was used to enhance the density to 4×10^{12} cm^{-3}. Within two seconds, approximately 5000 atoms were loaded in the dipole trap, and evaporation was done by adiabatically ramping down the trapping potential (Adams *et al.*, 1995).

In the Rice experiment, an atomic beam was Zeeman slowed, deflected and collimated, and passed through the center of a permanent-magnet trap (Tollet *et al.*, 1995). Doppler cooling provided the dissipation necessary to load the atoms into the trap. This resulted in 2×10^8 atoms at a density of 7×10^{10} cm^{-3} and a temperature of 200 μK. Evaporative cooling was done by ramping down an rf field, which, due to the high bias field of the trap, was in the gigahertz range. Trapping times of longer than 10 min allowed long cooling times, which were necessary due to the low initial density (Bradley *et al.*, 1995).

C. Comparison

Table III compiles the results of the experiments just mentioned. Although few careful comparisons with theory have been made so far, the table clearly shows that evaporative cooling has fulfilled its promises of efficiency and speed. In several cases, an order of magnitude decrease in the number of atoms resulted in a phase-space density increase of two to three orders of magnitude. In many experiments, this increase only required a few hundred elastic collision times. A rate of one order of magnitude phase-space density increase per second and an increase of the elastic collision rate by two orders of magnitude were also demonstrated. In agreement with our discussion in Section II, a large increase in phase-space density was only possible with constant or increasing collision rate.

VI. Outlook

The efficiency and versatility of evaporative cooling have been impressively demonstrated. Three groups have succeeded in reaching sufficient phase-space density to observe Bose–Einstein condensation of alkali atoms. In these experiments, evaporative cooling served to gain the last six orders of magnitude in phase-space density to the BEC transition line, and further evaporative cooling down to clouds with a condensate fraction of almost 100% was demonstrated (Davis *et al.*, 1995b; Anderson *et al.*, 1995). These results have triggered an enormous interest in evaporative cooling and

TABLE III
OVERVIEW OF EVAPORATIVE COOLING EXPERIMENTS

Atom	N^a	$n_0{}^a$ (cm^{-3})	T^a (K)	D^a	$\tau_{el}^{-1\,a}$ (sec^{-1})	t^b (sec)	$\gamma_{tot}{}^c$
$^1H^d$	2×10^{12}	5×10^{12}	0.05	2×10^{-6}	20	200	2.5
	3×10^{11}	8×10^{12}	3×10^{-3}	2×10^{-4}	7		
$^1H^e$	7×10^{12}	2×10^{13}	1.1×10^{-3}	2×10^{-3}	9	250	1.6
	3×10^{11}	8×10^{13}	1×10^{-4}	0.4	13		
$^1H^f$	5×10^{11}	3×10^{11}	0.2	2×10^{-8}	2	100	0.8
	4×10^{10}	4×10^{11}	0.06	1.5×10^{-7}	2		
$^1H^g$	8×10^{10}	5×10^{12}	0.011	2×10^{-5}	8	40	0.8
	7×10^{9}	4×10^{12}	3×10^{-3}	1.3×10^{-4}	4		
$^7Li^h$	2×10^{8}	7×10^{10}	2×10^{-4}	7×10^{-6}	3	300	1.7
	1×10^{5}	1.4×10^{12}	4×10^{-7}	2.6[l]	2		
$^{23}Na^i$	5×10^{3}	4×10^{12}	1.4×10^{-4}	1.2×10^{-4}	8×10^{2}	2	1.5
	5×10^{2}	6×10^{11}	4×10^{-6}	4×10^{-3}	20		
$^{23}Na^j$	1×10^{9}	1×10^{11}	2×10^{-4}	2×10^{-6}	23	7	1.9
	7×10^{5}	1.5×10^{14}	2×10^{-6}	2.6[l]	3×10^{3}		
$^{87}Rb^k$	4×10^{6}	4×10^{10}	9×10^{-5}	3×10^{-7}	5	70	3.0
	2×10^{4}	3×10^{12}	1.7×10^{-7}	2.6[l]	15		

[a] Upper row: initial value, lower row: final value, for number of atoms N, peak density n_0, temperature T, phase space density D, and peak elastic collision rate τ_{el}^{-1}.

[b] Duration of forced evaporation sweep t.

[c] The overall efficiency of evaporation $\gamma_{tot} = \log(D_f/D_i)/\log(N_i/N_f)$.

[d] Masuhara *et al.* (1988), MIT, cryogenic Ioffe–Pritchard (IP) trap, saddle-point evaporation.

[e] Doyle *et al.* (1991), MIT, cryogenic IP trap, saddle-point evaporation.

[f] Luiten *et al.* (1993), Amsterdam, cryogenic IP trap, saddle-point evaporation.

[g] Setija *et al.* (1993), Amsterdam, cryogenic IP trap, light-induced evaporation.

[h] Bradley *et al.* (1995), Rice, permanent-magnet IP trap, rf-induced evaporation.

[i] Adams *et al.* (1995), Stanford, crossed-dipole trap, evaporation by lowering the trap potential.

[j] Davis *et al.* (1995b), MIT, optically plugged, linear magnetic trap, rf-induced evaporation.

[k] Anderson *et al.* (1995), JILA, time-averaged, orbiting potential trap, rf-induced evaporation.

[l] Bose–Einstein condensation was reached; the number in this row reflect the situation at the transition point.

have led to a flurry of activity. We expect several parts of this chapter to be outdated soon by the rapid pace of future developments!

Doppler cooling was the method to reach 100 μK temperatures; polarization gradient cooling gave access to a few μK. Although an optical sub-recoil scheme holds the record for the lowest 1D temperature (3 nK), we regard evaporative cooling to be the most promising technique for the nano-Kelvin regime. Nano-Kelvin atoms are (as far as we know) the coldest matter in the universe. The step from micro-Kelvin to nano-Kelvin gave us access to new physics—quantum degenerate atomic gases. In contrast to many other cooling techniques, evaporative cooling is almost entirely classical, and it is amusing that it was this technique that revealed a hidden aspect of the quantum world.

Acknowledgments

We are grateful to M. R. Andrews, D. S. Durfee, D. M. Kurn, and M.-O. Mewes for valuable discussions and to J. Doyle for helpful comments on the manuscript. This work was supported by ONR, NSF, JSEP, and the Sloan Foundation. N.J.v.D. would like to acknowledge a Talent fellowship from "Nederlandse Organisatie voor Wetenschappelijk Onderzoek (NWO)" and a Fulbright fellowship from NACEE.

Note added in proof. The discussion on tightly confining magnetic traps in Section IV.B.1 was incomplete. The comparison between different traps assumed nearly isotropic confinement. An anisotropic Ioffe–Pritchard trap with tight radial confinement achieves a larger geometric mean of the three magnetic field curvatures than the TOP trap. The mean curvature is the figure of merit of a trap for evaporative cooling. Efficient evaporation and Bose–Einstein condensation in an optimized IP trap with only d.c. electromagnets have recently been obtained in our group. Evaporative cooling began with $\approx 2 \times 10^9$ atoms and reached BEC with 1.5×10^7 atoms after 15 to 25 sec (Mewes *et al.*, 1996).

References

Abraham, E. R. I., McAlexander, W. I., Sackett, C. A., and Hulet, R. G. (1995). *Phys. Rev. Lett.* **74**, 1315.

Adams, C. S., Lee, H. J., Davidson, N., Kasevich, M., and Chu, S. (1995). *Phys. Rev. Lett.* **74**, 3577.

Agosta, C. C. Silvera, I. F., Stoof, H. T. C., and Verhaar, B. J. (1989). *Phys. Rev. Lett.* **62**, 2361.

Aminoff, C. G., Steane, A. M., Bouyer, P., Desbiolles, P., Dalibard, J., and Cohen-Tannoudji, C. (1993). *Phys. Rev. Lett.* **71**, 3083.

Anderson, M. H., Petrich, W., Ensher, J. R., and Cornell, E. A. (1994). *Phys. Rev. A* **50**, R3597.

Anderson, M. H., Ensher, J. R., Matthews, M. R., Wieman, C. E., and Cornell, E. A. (1995). *Science* **269**, 198.

Aspect, A., Arimondo, E., Kaiser, R., Vansteenkiste, N., and Cohen-Tannoudji, C. (1988). *Phys. Rev. Lett.* **61**, 826.

Bagnato, V. S., Lafyatis, G. P., Martin, A. G., Raab, E. L., Ahmad-Bitar, R. N., and Pritchard, D. E. (1987). *Phys. Rev. Lett.* **58**, 2194.

Bardou, F., Emile, O., Courty, J.-M., Westbrook, C. I., and Aspect, A. (1992). *Europhys. Lett.* **20**, 681.

Bergeman, T., Erez, G., and Metcalf, H. (1987). *Phys. Rev. A* **35**, 1535.

Bergeman, T., McNicholl, P., Kycia, J., Metcalf, H., and Balazs, N. L. (1989). *J. Opt. Soc. Am. B* **6**, 2249.

Berman, L. D. (1961). "Evaporative Cooling of Circulating Water." Pergamon, New York.

Boesten, H. M. J. M., Moerdijk, A. J., Verhaar, B. J. (1996). *Phys. Rev. A* **54**, R29.

Bradley, C. C., Sackett, C. A., Tollet, J. J., and Hulet, R. G. (1995). *Phys. Rev. Lett.* **75**, 1687.

Cable, A., Prentiss, M., and Bigelow, N. P. (1990). *Opt. Lett.* **15**, 507.

Castin, Y., Dalibard, J., and Cohen-Tannoudji, C. (1995). In "Bose-Einstein Condensation" (A. Griffin, D. W. Snoke, and S. Stringari, eds.), BEC-93, p. 173. Cambridge Univ. Press, Cambridge, UK.

Cesar, C. L., Fried, D. G., Killian, T. C., Polcyn, A. D., Sandberg, J. C., Yu, I. A., Greytak, T. J., Kleppner, D., and Doyle, J. M. (1996). *Phys. Rev. Lett.* (in press).

Chen, J., Story, J. G., Tollet, J. J., and Hulet, R. G. (1992). *Phys. Rev. Lett.* **69**, 1344.

Chu, S., Bjorkholm, J. E., Ashkin, A., and Cable, A. (1986). *Phys. Rev. Lett.* **57**, 314.

Cirac, J. I. and Lewenstein, M. (1995). *Phys. Rev. A* **52**, 4737.

Coakley, K. J. (1996). Submitted.

Cohen-Tannoudji, C., Dupont-Roc, J., and Grynberg, G. (1992). "Atom-Photon Interactions." Wiley, New York.

Cornell, E. A., Monroe, C., and Wieman, C. E. (1991). *Phys. Rev. Lett.* **67**, 2439.

Davidson, N., Lee, H.-J., Kasevich, M., and Chu, S. (1994). *Phys. Rev. Lett.* **72**, 3158.

Davidson, N., Lee, H. J., Adams, C. S., Kasevich, M., and Chu, S. (1995). *Phys. Rev. Lett.* **74**, 1311.

Davis, K. B., Mewes, M. O., Joffe, M. A., and Ketterle, W. (1994). *Int. Conf. At. Phys. 14th,* Boulder, CO, 1994, Book Abst., 1-M3.

Davis, K. B., Mewes, M.-O., Joffe, M. A., Andrews, M. R., and Ketterle, W. (1995a). *Phys. Rev. Lett.* **74**, 5202.

Davis, K. B., Mewes, M.-O., Andrews, M. R., van Druten, N. J., Durfee, D. S., Kurn, D. M., and Ketterle, W. (1995b). *Phys. Rev. Lett.* **75**, 3969.

Davis, K. B., Mewes, M.-O., and Ketterle, W. (1995c). *Appl. Phys. [Part] B* **B60**, 155.

Doyle, J. (1996). Private communication.

Doyle, J. M. (1991). Ph.D. Thesis, Massachusetts Institute of Technology, Cambridge, MA.

Doyle, J. M., Sandberg, J. C., Masuhara, N., Yu, I. A., Kleppner, D., and Greytak, T. J. (1989). *J. Opt. Soc. Am. B* **6**, 2244.

Doyle, J. M., Sandberg, J. C., Yu, I. A., Cesar, C. L., Kleppner, D., and Greytak, T. J. (1991). *Phys. Rev. Lett.* **67**, 603.

Doyle, J. M., Sandberg, J. C., Yu, I. A., Cesar, C. L., Kleppner, D., and Greytak, T. J. (1994). *Physica B (Amsterdam)* **194–196**, 13.

Doyle, J. M., Friedrich, B., Kim, J., and Patterson, D. (1995). *Phys. Rev. A* **52**, R2515.
Drewsen, M., Laurent, P., Nadir, A., Santarelli, G., Clairon, A., Castin, Y., Grison, D., and Salomon, C. (1994). *Appl. Phys. [Part] B* **B59**, 283.
Dum, R., Marte, P., Pellizzari, T., and Zoller, P. (1994). *Phys. Rev. Lett.* **73**, 2829.
Ertmer, W., Blatt, R., Hall, J. L., and Zhu, M. (1985). *Phys. Rev. Lett.* **54**, 996.
Esslinger, T., Sander, F., Weidemüller, M., Hemmerich, A., and Hänsch, T. W. (1996). *Phys. Rev. Lett.* **76**, 2432.
Evans, R. G., Kroeger, M. W., and Mahan, M. O. (1995). *App. Eng. Agric.* **11**, 93.
Fedichev, P. O., Reynolds, M. W., Rahmanov, U. M., and Shlyapnikov, G. V. (1996a). *Phys. Rev. A* **53**, 1447.
Fedichev, P. O., Reynolds, M. O., and Shlyapnikov, G. V. (1996b). Submitted.
Frerichs, V., Kaenders, W., and Meschede, D. (1992). *Appl. Phys. [Part] B* **B55**, 242.
Friend, D. G., and Etters, R. D. (1980). *J. Low Temp. Phys.* **39**, 409.
Gardner, J. R., Cline, R. A., Miller, J. D., Heinzen, D. J., Boesten, H. M. J. M., and Verhaar, B. J. (1995). *Phys. Rev. Lett.* **74**, 3764.
Gott, Y. V., Ioffe, M. S., and Tel'kovskii, V. G. (1962). *Nucl. Fusion, Suppl.*, Pt. 3, 1045 and 1284.
Greytak, T. J. (1995). *In* "Bose-Einstein Condensation" (A. Griffin, D. W. Snoke, and S. Stringari, eds.), BEC-93, p. 131. Cambridge Univ. Press, Cambridge, UK.
Greytak, T. J., and Kleppner, D. (1984). *In* "New Trends in Atomic Physics" (G. Grynberg and R. Stora, eds.), Les Houches Summer School, 1982, p. 1125. North-Holland Publ., Amsterdam.
Han, D. J., Mochizuki, K., Gardner, J. R., and Heinzen, D. J. (1995). *Bull. Am. Phys. Soc.* [2] **40**, 1348.
Heinzen, D. J. (1995). *At. Phys.* **14**, 369.
Helmerson, K., Martin, A., and Pritchard, D. E. (1992a). *J. Opt. Soc. Am. B* **9**, 483.
Helmerson, K., Martin, A., and Pritchard, D. E. (1992b). *J. Opt. Soc. Am. B* **9**, 1988.
Hemmerich, A., Weidemüller, M., Esslinger, T., Zimmermann, C., and Hänsch, T. W. (1995). *Phys. Rev. Lett.* **75**, 37.
Hess, H. (1985). *Bull. Am. Phys. Soc.* [2] **30**, 854.
Hess, H. F. (1986). *Phys. Rev. B: Condens. Matter* [3] **34**, 3476.
Hess, H. F., Bell, D. A., Kochanski, G. P., Kleppner, D., and Greytak, T. J. (1984). *Phys. Rev. Lett.* **52**, 1520.
Hess, H., Kochanski, G. P., Doyle, J. M., Masuhara, N., Kleppner, D., and Greytak, T. J. (1987). *Phys. Rev. Lett.* **59**, 672.
Hijmans, T. W., Luiten, O. J., Setija, I. D., and Walraven, J. T. M. (1989). *J. Opt. Soc. Am B* **6**, 2235.
Hijmans, T. W., Kagan, Y., Shlyapnikov, G. V., and Walraven, J. T. M. (1993). *Phys. Rev. B: Condens. Matter* [3] **48**, 12886.
Holland, M., Burnett, K., Gardiner, C., Cirac, J. I., and Zoller, P. (1996a). *Phys. Rev. A.*, to appear.
Holland, M., Williams, J., Coakley, K., and Cooper, J. (1996b). *Quantum Semiclass. Opt.* **8**, 571.
Huang, K. (1987). "Statistical Mechanics," 2nd ed. Wiley, New York.
Imajo, H., Hayasaka, K., Ohmukai, R., Tanaka, U., Watanabe, M., and Urabe, S. (1996). *Phys. Rev. A* **53**, 122.
Joffe, M. A., Ketterle, W., Martin, A., and Pritchard, D. E. (1993). *J. Opt. Soc. Am. B* **10**, 2257.
Kagan, Y. (1995). *In* "Bose-Einstein Condensation" (A. Griffin, D. W. Snoke, and S. Stringari, eds.), BEC-93, p. 202. Cambridge Univ. Press, Cambridge, UK.

Kagan, Y., Svistunov, B. V., and Shlyapnikov, G. V. (1985). *JETP Lett.* (*Engl. Transl.*) **42**, 209.
Kasevich, M. A. (1995). *Bull. Am. Phys. Soc.* [2] **40**, 1270.
Kasevich, M., and Chu, S. (1992). *Phys. Rev. Lett.* **69**, 1741.
Kastberg, A., Phillips, W. D., Rolston, S. L. Spreeuw, R. J. C., and Jessen, P. S. (1995). *Phys. Rev. Lett.* **74**, 1542.
Katori, H. and Shimizu, F. (1994). *Phys. Rev. Lett.* **73**, 2555.
Ketterle, W., Davis, K. B., Joffe, M. A., Martin, A., and Pritchard, D. E. (1993). Invited oral presentation at the Annual Meeting of the Optical Society of America, Toronto, Canada, October 3–8.
Ketterle, W., and Pritchard, D. E. (1992). *Appl. Phys.* [*Part*] *B* **B54**, 403.
Ketterle, W., Davis, K. B., Joffe, M. A., Martin, A., and Pritchard, D. E. (1993). *Phys. Rev. Lett.* **70**, 2253.
Koelman, J. M. V. A., Stoof, H. T. C., and Verhaar, B. J. (1987). *Phys. Rev. Lett.* **59**, 676.
Kügler, K.-J., Moritz, K., Paul, W., and Trinks, U. (1985). *Nuc. Instrum. Methods Phys. Res.* **228**, 240.
Larson, D. J., Bergquist, J. C., Bollinger, J. J., Itano, W. M., and Wineland, D. J. (1986). *Phys. Rev. Lett.* **57**, 70.
Lawall, J., Bardou, F., Saubamea, B., Shimizu, K., Leduc, M., Aspect, A., and Cohen-Tannoudji, C. (1994). *Phys. Rev. Lett.* **73**, 1915.
Lawall, J., Kulin, S., Saubamea, B., Bigelow, N., Leduc, M., and Cohen-Tannoudji, C. (1995). *Phys. Rev. Lett.* **75**, 4194.
Lee, H. J., Adams, C. S., Kasevich, M., and Chu, S. (1996). *Phys. Rev. Lett.* **76**, 2658.
Lee, H. J., Adams, C. S., Davidson, N., Young, B., Weitz, M., Kasevich, M., and Chu, S. (1995). *At. Phys.* **14**, 258.
Lemonde, P., Morice, O., Peik, E., Reichel, J., Perrin, H., Hänsel, W., and Salomon, C. (1996). *Europhys. Lett.* **32**, 555.
Lett, P. D., Julienne, P. S., and Phillips, W. D. (1995). *Annu. Rev. Phys. Chem.* **46**, 423.
Lett, P. D., Phillips, W. D., Rolston, S. L., Tanner, C. E., Watts, R. N., and Westbrook, C. I. (1989). *J. Opt. Soc. Am. B* **6**, 2084.
Lovelace, R. V. E., Mahanian, C., Tommila, T. J., and Lee, D. M. (1985). *Nature* (*London*) **318**, 30.
Luiten, O. J. (1993). Ph.D. Thesis, University of Amsterdam.
Luiten, O. J., Werij, H. G. C., Setija, I. D., Reynolds, M. W., Hijmans, T. W., and Walraven, J. T. M. (1993). *Phys. Rev. Lett.* **70**, 544.
Luiten, O. J., Werij, H. G. C., Reynolds, M. W., Setija, I. D., Hijmans, T. W., and Walraven, J. T. M. (1994). *Physica B* (*Amsterdam*) **194–196**, 897.
Luiten, O. J., Reynolds, M. W., and Walraven, J. T. M. (1996). *Phys. Rev. A* **53**, 381.
Marcassa, L., Muniz, S., de Queiroz, E., Zilio, S., Bagnato, V., Weiner, J., Julienne, P. S., and Suominen, K.-A. (1994). *Phys. Rev. Lett.* **73**, 1911.
Martin, A. G., Helmerson, K., Bagnato, V. S., Lafyatis, G. P., and Pritchard, D. E. (1988). *Phys. Rev. Lett.* **61**, 2431.
Masuhara, N., Doyle, J. M., Sandberg, J. C., Kleppner, D., Greytak, T. J., Hess, H. F., and Kochanski, G. P. (1988). *Phys. Rev. Lett.* **61**, 935.
Mewes, M.-O., Andrews, M. R., van Druten, N. J., Kurn, D. M., Durfee, D. S., and Ketterle, W. (1996). *Phys. Rev. Lett.*, in press.
Migdall, A. L., Prodan, J. V., Phillips, W. D., Bergeman, T. H., and Metcalf, H. J. (1985). *Phys. Rev. Lett.* **54**, 2596.
Miller, J. D., Cline, R. A., and Heinzen, D. J. (1993). *Phys. Rev. A* **47**, R4567.
Moerdijk, A. J., and Verhaar, B. J. (1994). *Phys. Rev. Lett.* **73**, 518.
Moerdijk, A. J., Verhaar, B. J., and Axelsson, A. (1995). *Phys. Rev. A* **51**, 4852.

Moerdijk, A. J., and Verhaar, B. J. (1996). *Phys. Rev. A* **53**, R19.
Moerdijk, A. J., Boesten, H. M. J. M., and Verhaar, B. J. (1996a). *Phys. Rev. A* **53**, 916.
Moerdijk, A. J., Verhaar, B. J., and Nagtegaal, T. M. (1996b). *Phys. Rev. A* **53**, 4343.
Monroe, C. R., Swann, W., Robinson, H., and Wieman, C. E. (1990). *Phys. Rev. Lett.* **65**, 1571.
Monroe, C. R., Cornell, E. A., Sackett, C. A., Myatt, C. J., and Wieman, C. E. (1993). *Phys. Rev. Lett.* **70**, 414.
Newbury, N. R., and Wieman, C. E. (1996). *Am. J. Phys.* **64**, 18.
Newbury, N. R., and Myatt, C. J., Cornell, E. A., and Wieman, C. E. (1994). *Phys. Rev. Lett.* **74**, 2196.
Newbury, N. R., Myatt, C. J., and Wieman, C. E. (1995). *Phys. Rev. A* **51**, R2680.
Nolan, P. J., and Twin, P. J. (1988). *Annu. Rev. Nucl., Part. Sci.* **38**, 533.
Pellizzari, T., and Ritsch, H. (1995). *Europhys. Lett.* **31**, 133.
Petrich, W., Anderson, M. H. Ensher, J. R., and Cornell, E. A. (1994a). *J. Opt. Soc. Am. B* **11**, 1332.
Petrich, W., Anderson, M. H., Ensher, J. R., and Cornell, E. A. (1994b). *Int. Conf. At. Phys., 14th,* Boulder, CO, 1994, Book Abstr. 1M-7.
Petrich, W., Anderson, M. H., Ensher, J. R., and Cornell, E. A. (1995). *Phys. Rev. Lett.* **74**, 3352.
Phillips, W. D. (1992). *Proc. Int. Sch. Phys. "Enrico Fermi"* **118**, 289.
Phillips, W. D., Prodan, J. V., and Metcalf, H. J. (1985). *J. Opt. Soc. Am. B* **2**, 1751.
Pritchard, D. E. (1983). *Phys. Rev. Lett.* **51**, 1336.
Pritchard, D. E., and Ketterle, W. (1992). *Proc. Int. Sch. Phys. "Enrico Fermi"* **118**, 473.
Pritchard, D. E., Helmerson, K., Bagnato, V. S., Lafyatis, G. P., and Martin, A. G. (1987). *Springer Ser. Opt. Sci.* **55**, 68.
Pritchard, D. E., Helmerson, K., and Martin, A. G. (1989). *At. Phys.* **11** 179.
Quadt, R., Wiseman, H. M., and Walls, D. F. (1996). *Phys. Lett. A*, to appear.
Raab, E. L., Prentiss, M., Cable, A., Chu, S., and Pritchard, D. E. (1987). *Phys. Rev. Lett.* **59**, 2631.
Reichel, J., Bardou, F., Dahan, M. B., Peik, E., Rand, S., Salomon, C., and Cohen-Tannoudji, C. (1995). *Phys. Rev. Lett.* **75**, 4575.
Ricci, L., Zimmermann, C., Vuletić, V., and Hänsch, T. W. (1994). *Appl. Phys.* [*Part*] *B* **B59**, 195.
Riis, E., and Barnett, S. M. (1993). *Europhys. Lett.* **21**, 533.
Rooijakkers, W., Hogervorst, W., and Vassen, W. (1995). *Phys. Rev. Lett.* **74**, 3348.
Rubbmark, J. R., Kash, M. M., Littman, M. G., and Kleppner, D. (1981). *Phys. Rev. A* **23**, 3107.
Sanchez-Villicana, V., Gensemer, S. D., Tan, K. Y. N., Kumarakrishnan, A., Dinneen, T. P., Süptitz, W., and Gould, P. L. (1995). *Phys. Rev. Lett.* **74**, 4619.
Santos, M. S., Nussenzveig, P., Marcassa, L. G., Helmerson, K., Flemming, J., Zilio, S. C., and Bagnato, V. S. (1996). *Phys. Rev. A* **52**, R4340.
Schwinger, J. (1937). *Phys. Rev.* **51**, 648.
Setija, I. D. (1995). Ph.D. Thesis, University of Amsterdam.
Setija, I. D., Werij, H. G. C., Luiten, O. J., Reynolds, M. W., Hijmans, T. W., and Walraven, J. T. M. (1993). *Phys. Rev. Lett.* **70**, 2257.
Shimizu, F., and Morinaga, M. (1992). *Jpn. J. Appl. Phys.* **31**, L1721.
Shlyapnikov, G. V., Walraven, J. T. M., and Surkov, E. L. (1993). *Hyperfine Interact.* **76**, 31.
Shlyapnikov, G. V., Walraven, J. T. M., Rahmanov, U. M., and Reynolds, M. W. (1994). *Phys. Rev. Lett.* **73**, 3247.
Silvera, I. F. (1995a). *J. Low Temp. Phys.* **101**, 49.

Silvera, I. F. (1995b). *In* "Bose-Einstein Condensation" (A. Griffin, D. W. Snoke, and S. Stringari, eds.), BEC-93, p. 160. Cambridge Univ. Press, Cambridge, UK.
Silvera, I. F., and Reynolds, M. (1991). *Physica B (Amsterdam)* **169**, 449.
Silvera, I. F., and Reynolds, M. (1992). *J. Low Temp. Phys.* **87**, 343.
Silvera, I. F., and Walraven, J. T. M. (1986). *Prog. Low Temp. Phys.* **10**, 139.
Snoke, D. W., and Wolfe, J. P. (1989). *Phys. Rev. B: Condens. Matter* [3] **39**, 4030.
Snoke, D. W., Rühle, W. W., Lu, Y.-C., and Bauser, E. (1992). *Phys. Rev. B: Condens. Matter* [3] **45**, 10979.
Spitzer, L., Jr. (1987). "Dynamical Evolution of Globular Clusters." Princeton Univ. Press, Princeton, NJ.
Spreeuw, R. J. C., Gerz, C., Goldner, L. S., Phillips, W. D., Rolston, S. L., Westbrook, C. I., Reynolds, M. W., and Silvera, I. F. (1994). *Phys. Rev. Lett.* **72**, 3162.
Stoof, H. T. C. (1995). *In* "Bose-Einstein Condensation" (A. Griffin, D. W. Snoke, and. S. Stringari, eds.), BEC-93, p. 226. Cambridge Univ. Press, Cambridge, UK.
Stoof, H. T. C., Koelman, J. M. V. A., and Verhaar, B. J. (1988). *Phys. Rev. B: Condens. Matter* [3] **38**, 4688.
Stoof, H. T. C., Houbiers, M., Sackett, C. A., and Hulet, R. G. (1996). *Phys. Rev. Lett.* **76**, 10.
Süptitz, W., Wokurka, G., Strauch, F., Kohns, P., and Ertmer, W. (1994). *Opt. Lett.* **19**, 1571.
Surkov, E. L., Walraven, J. T. M., and Shlyapnikov, G. V. (1994). *Phys. Rev. A* **49**, 4778.
Surkov, E. L., Walraven, J. T. M., and Shlyapnikov, G. V. (1996). *Phys. Rev. A* **53**, 3403.
Takekoshi, T., Yeh, J. R., and Knize, R. J. (1996). *Opt. Lett.* **21**, 77.
Thompson, R., Steinberg, A., Helmerson, K., and Phillips, W. D. (1995). *Res. Conf. Bose-Einstein Condens.*, Mont Ste Odile, France, *1995*, Book Abstr. p. 74.
Tiesinga, E., Kuppens, S. J. M., Verhaar, B. J., and Stoof, H. T. C. (1991). *Phys. Rev. A* **43**, 5188.
Tiesinga, E., Moerdijk, A. J., Verhaar, B. J., and Stoof, H. T. C. (1992). *Phys. Rev. A* **46**, R1167.
Tiesinga, E., Verhaar, B. J., and Stoof, H. T. C. (1993). *Phys. Rev. A* **47**, 4114.
Tollet, J. J., Bradley, C. C., Sackett, C. A., and Hulet, R. G. (1995). *Phys. Rev. A* **51**, R22.
Tommila, T. (1986). *Europhys. Lett.* **2**, 789.
Townsend, C. G., Edwards, N. H., Cooper, C. J., Zetie, K. P., Foot, C. J., Steane, A. M., Szriftgiser, P., Perrin, H., and Dalibard, J. (1995). *Phys. Rev. A* **52**, 1423.
Townsend, C. G., Edwards, N. H., Zetie, K. P., Cooper, C. J., Rink, J., and Foot, C. J. (1996). *Phys. Rev. A* **53**, 1702.
van Roijen, R., Berkhout, J. J., Jaakkola, S., and Walraven, J. T. M. (1988). *Phys. Rev. Lett.* **61**, 931.
Verhaar, B. J. (1995). *At. Phys.* **14**, 351.
Verhaar, B. J., Gibble, K., and Chu, S. (1993). *Phys. Rev. A* **48**, R3429.
Walhout, M., Sterr, U., Orzel, C., Hoogerland, M., and Rolston, S. L. (1995). *Phys. Rev. Lett.* **74**, 506.
Walker, T., and Feng, P. (1994). *Adv. At. Mol. Opt. Phys.* **34**, 125.
Walker, T., Sesko, D., and Wieman, C. (1990). *Phys. Rev. Lett.* **64**, 408.
Walraven, J. T. M. (1996). *Proc. Scott. Univ. Summer Sch. Phys.* **44**.
Walraven, J. T. M., and Hijmans, T. W. (1994). *Physica B (Amsterdam)* **197**, 417.
Willems, P. A., and Libbrecht, K. G. (1995). *Phys. Rev. A* **51**, 1403.
Wing, W. H. (1984). *Prog. Quantum Electron.* **8**, 181.
Wiseman, H., Martins, A., and Walls, D. (1996). *Quantum Semiclass. Opt.* **8**, 737.
Wu, H., and Foot, C. J. (1996). To be published.